GEOLOGICA CARPATHICA, FEBRUARY 2013, 64, 1, 39–62 doi: 10.2478/geoca-2013-0003

Paleoenvironments during the Rhaetian transgression and the colonization history of marine biota in the Fatric Unit (Western Carpathians)

JOZEF MICHALÍK[1], OTÍLIA LINTNEROVÁ[2], PATRYCJA WÓJCIK-TABOL[3], ANDRZEJ GAŹDZICKI[4], JACEK GRABOWSKI[5], MARIÁN GOLEJ[1], VLADIMÍR ŠIMO[1] and BARBARA ZAHRADNÍKOVÁ[6]

[1]Geological Institute, Slovak Academy of Sciences, Dúbravská cesta 9, P.O.Box 106, 840 05 Bratislava, Slovak Republic; geolmich@savba.sk; geolmgol@savba.sk; geolsimo@savba.sk
[2]Department of Geology and Mineral Deposits, Faculty of Natural Sciences, Comenius University, Mlynská dolina G1, 842 15 Bratislava, Slovak Republic; lintnerova@fns.uniba.sk
[3]Department of Geological Sciences, Jagiellonian University, Oleandry Str. 2a (room 109), 30-063 Kraków, Poland
[4]Institute of Paleobiology, Polish Academy of Sciences, Twarda 51/55, 00-818 Warszawa, Poland; gazdzick@twarda.pan.pl
[5]Polish Geological Institute, National Research Institute, Rakowiecka 4, 00-975 Warszawa, Poland; jacek.grabowski@pgi.gov.pl
[6]Slovak National Museum, Natural Science Museum, Vajanského nábrežie 2, P.O.Box 13, 810 06 Bratislava, Slovak Republic; barbara.zahradnikova@snm.sk

(Manuscript received May 23, 2012; accepted in revised form September 18, 2012)

Abstract: Terminal Triassic environmental changes are characterized by an integrated study of lithology, litho- and cyclostratigraphy, paleontology, mineralogy, geochemistry and rock magnetism in the Tatra Mts. The Carpathian Keuper sequence was deposited in an arid environment with only seasonal rivers, temporal lakes and swamps with scarce vegetation. Combination of a wide range of $\delta^{18}O$ values (–0.7 to +2.7) with negative $\delta^{13}C$ values documents dolomite precipitation either from brackish or hypersaline lake water, or its derivation from pore water comparably to the Recent Coorong B-dolostone. Negative $\delta^{13}C$ values indicate microbial C productivity. Rhaetian transgressive deposits with restricted *Rhaetavicula* fauna accumulated in nearshore swamps and lagoons. Associations of foraminifers, bivalves and sharks in the Zliechov Basin were controlled by physical factors. Bivalve mollusc biostromes were repetitively destroyed by storms, and temporary firm bottoms were colonized by oysters and burrowers. Subsequent black shale deposition recorded input of eolian dust. Bottom colonization by pachyodont bivalves, brachiopod and corals started much later, during highstand conditions. Facies evolution also revealed by geochemical data, C and O isotope curves reflect eustatic and climatic changes and help reconstruct the evolution of Rhaetian marine carbonate ramp. The Fatra Formation consists of 100 kyr eccentricity and 40 kyr obliquity cycles; much finer rhythmicity may record monsoon-like climatic fluctuations. Fluvial and eolian events were indicated by analysis of grain size and content of clastic quartz, concentrations of foraminiferal (*Agathammina*) tests in thin laminae indicates marine ingression events. Magnetic susceptibility (MS) variations reflect the distribution of authigenic and detrital constituents in the sequence. Increasing trend of MS correlates with the regressive Carpathian Keuper sequence and culminates within the bottom part of the Fatra Formation. Decreasing trend of MS is observed upwards the transgressive deposits of the Fatra Formation.

Key words: uppermost Triassic, Western Tethys, Slovakia, sedimentology, sequence stratigraphy, geochemistry, marine fauna.

Introduction

In spite of numerous previous works devoted to the terminal Triassic sedimentary and biotic evolution, precise dating and event successions during the Rhaetian transgression have remained little known since the establishment of the "Avicula contorta Schichten" by Winkler (1859). We selected the Kardolína section situated on a steep western slope of the Mt Pálenica (NNE of the Tatranská Kotlina village) in the Belianske Tatry Mts (GPS coordinate 49°14′997″N: 20°18′894″E, Figs. 1 and 2) as the most continuous section of the Rhaetian Fatra Formation in the former Zliechov Basin (Fatric Unit), the upper part of which has been studied by Michalík et al. (2007). The sedimentary record was analysed by sedimentological, biostratigraphical, geochemical and magnetic susceptibility methods. Detailed study of cyclostratigraphy enabled us to assess periodicity estimate, duration of sedimentary cycles, and climate proxies. Preservation of primary magnetic record is promising for future detailed study of magnetostratigraphy.

Geological setting

Terrigenous Carpathian Keuper was deposited during the Carnian and Norian on extensive lowlands adjacent to North Tethyan shelves. Limanowski (1903) interpreted its environment as a continental domain. Turnau-Morawska (1953) regarded variegated shales, sandstones and dolostones as marine

sediments with fluvial intercalations. Borza (1959) postulated a primary character of Keuper dolostones. Gaździcki et al. (1979) recognized three informal members in the sequence: the basal member with clastic intercalations, the middle one with prevalence of variegated claystones and the upper member, that consists of claystone/dolostone alternation. They stressed the terrigenous nature of the palynoflora in the claystones (*Gliscopollis*/*Classopollis* assemblage), whereas the dolostone intercalations yielded more diversified associations of pollen, spores and marine acritarchs. Al-Juboury & Ďurovič (1992, 1996) supposed hypersaline conditions of the Keuper dolomite formation. Rychliński (2008) and Jaglarz (2010) distinguished several depositional environments: mudflats, fluvial, sabkha, and flat marine, evolving under fluctuating wet — semi-arid and arid climate.

Fig. 1. Location of the Kardolína section on the slope of Mt Lendacká Pálenica near Tatranská Kotlina in the Belianske Tatry Mts.

Fig. 2. Rocky outcrop above the Kardolína gamekeeper's cottage on the western slope of Mt Pálenica. Right corner: contact of the Carpathian Keuper with the Fatra Formation.

During the latest Triassic, dry emerged plains were inundated by shallow sea flooding the opening tensional depressions (Michalík 1993). Transgression was not a short and uniform event. Instead, sea reached different parts of the area in several pulses (Gaździcki & Iwanow 1983). Bioclastic, shelly, and oolitic limestones, marlstones, dolostones and marls were laid down in salt marshes, littoral banks, carbonate ramps, up to deeper neritic slope of the almost 300 km long and 100 km wide tensional semi-closed shallow marine basin (the Fatric Zone of the central Western Carpathians; Michalík 1977; Michalík et al. 2007). The carbonate ramp faced a deeper, dysoxic basin.

The new biotope created by the Rhaetian marine transgression was colonized by pioneer organisms (foraminifers, bivalves and fish). The Kardolína section is more suitable for detailed study of this process than other less complete sections in the Fatric Unit (Michalík 1977, 1979, 1982; Michalík et al. 2007). Benthic associations were dominated by bivalves *Placunopsis alpina* (Winkler) and *Rhaetavicula contorta* (Portlock), gastropods, and foraminifers *Agathammina austroalpina* Kristan-Tollmann & Tollmann (Michalík & Jendrejáková 1978; Michalík 1978a). Upper Triassic bivalve faunas have been studied by Allasinaz (1972), Kollárová-Andrusovová & Kochanová (1973), Hallam (1981), Golebiowski (1991), Ivimey-Cook et al. (1999) and Hautmann (2001). Fish remains (single shark and actinopterygian teeth and scales) were reported by Gaździcki (1974), Duffin & Gaździcki (1977), Michalík (1977, 1979), and by Gaździcki et al. (1979). More mature communities were represented by brachiopods *Rhaetina gregaria* (Suess), *Zugmayerella uncinata* (Schafhäutl), *Austrirhynchia cornigera* (Suess) — (Michalík 1975, 1978b, 1980); foraminifers *Aulotortus friedli* (Kristan-Tollmann), *Glomospirella pokornyi* (Salaj), *Triasina hantkeni* Majzon — (Gaździcki 1983); and/or by corals *Retiophyllia paraclathrata* Roniewicz, *Rhaetiastraea tatrica* Roniewicz, etc. — (Roniewicz & Michalík 1998); sponges, algae and hydrozoans inhabiting the carbonate ramp. However, evolution of any true reef bio-constructions was prevented by storms and sea-level fluctuations (Michalík 1980, 1982). The palynofacies characterized by *Ricciisporites tuberculatus* Lundblad was dominated by terrestrial components and by a high amount of phytoclasts. Its marine fraction dominated by the dinoflagellate cyst *Rhaetogonyaulax rhaetica* Sarjeant points to a very shallow marine depositional environment (Götz in Michalík et al. 2007). Microflora from the upper part of the Fatra Formation resembles associations of the *Ricciisporites tuberculatus* Zone of the Polish zonation and of the *Ricciisporites–Polydiisporites* Zone of the SE North Sea Basin,

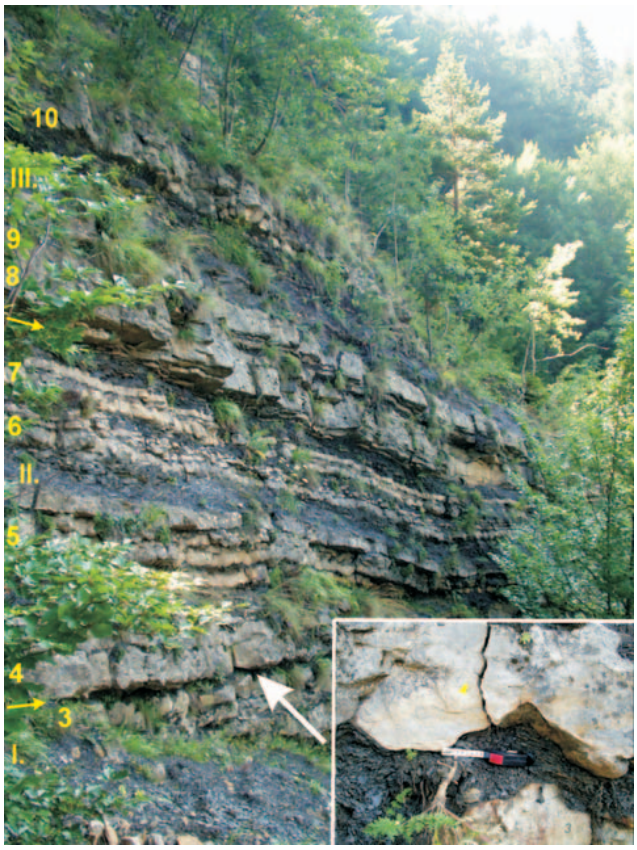

Fig. 3. Lower part of the Fatra Formation in the Kardolína section formed by the "tempestite cycle" (Beds 3 to 10). Right lower corner: the Bed 4 with loadcasts on the base.

both indicating middle to late Rhaetian age (Ruckwied & Götz 2009).

Material and methods

In the well exposed, 122 m thick Kardolína section, we concentrated on its lower part (69 m, Fig. 3), where 42 dolostone and 103 limestone layers were distinguished and numbered. Basal beds of the Fatra Formation were designated as the "zero interval" (however, later, it was proved that the uppermost layers of the Carpathian Keuper bear signs of marine origin and the Bed –5 consists of first limestone biomicrite). Samples were taken by the bed by bed method, but thicker layers were sampled more densely. The Carpathian Keuper sequence was numbered downwards, thus in opposite order to the Fatra Formation, but with a "minus" mark.

From each sample, a thin section has been made for microscopic study. Allochem contents were evaluated from percentages obtained under an optical microscope both with use of estimation tables (Bacelle & Bosellini 1965; Schäfer 1969; Soudant 1972; Michalík et al. 2007), and of the NICON NIS-Elements BR System for screen analysis. Micrite, sparite, bioclast and lithic clast contents, as well as the average size of clastic quartz grains were measured (Fig. 4). Micrite and sparite were compared as antagonistic elements (as the Reijmer 1968) in Fig. 5.

Total abundance of major oxides, several trace elements, and REE were analysed in the ACME Analytical Laboratories, Ltd in Vancouver, Canada, in 12 samples. REE were normalized to the Post-Archaean Australian Shale = PAAS (Taylor & McLennan 1985). The Eu/Eu* ratios (Eu anomaly values) were calculated using $Eu_{PAAS}/Sm_{PAAS} \times Gd_{PAAS})^{0.5}$ ratio. The inter-elemental relationship has been evaluated using the Pearson's Correlation Factor.

The total organic carbon content (TOC) and total inorganic carbon content (TIC) was measured on C-MAT 5500 Ströhlein device in the laboratory of the Geological Institute of the Slovak Academy of Sciences in Banská Bystrica. TIC content was re-calculated on the content of $CaCO_3$ in 35 selected samples.

O and C isotope ratios were analysed in 65 samples in CO_2 after the standard dissolution of samples in 100% phosphoric acid on the Finigan MAT-2 Mass Spectrometer in the laboratories of both the Czech Geological Institute in Prague and the Institute of Paleobiology of the Polish Academy of Sciences in Warsaw. The results are presented in standard delta notation (δ) in permil (‰) relative to the Vienna International Isotopic Standard (VPDB) with 0.01‰ accuracy.

The carbon isotope ratio of C_{org} was analysed after carbonate dissolution in 8 samples enriched to TOC. The $\delta^{13}C$ measurements were performed in the Czech Geological Survey Laboratory in Prague by flash combustion in a Fisons 1108 Elemental Analyzer coupled with Mat 251 Isotope Ratio Mass Spectrometer in a continuous flow regime. The sample size was adjusted to contain a sufficient amount of C_{org} to obtain external reproducibility of 0.15 ‰ for $\delta^{13}C_{org}$ for all types of samples with NBS22 as the reference material. Isotope data are reported in the usual delta (δ) notation relative to VPDB.

Foraminiferal tests were studied in thin sections by optical microscope. Bivalve molluscs were prepared mechanically by vibro-tool, they were coated with ammonium chloride prior to photographying. Shark teeth were collected mainly from the upper part of Beds 2.2 and 2.3, single fish teeth and vertebrae from insoluble residue after dissolving samples 2.3, 3.4, 13/14 and 14 in diluted acetic acid. Descriptive terminology of *Chondrichthyes* is based on Cappetta (1987) and fish terminology is based on Swift & Martill (1999). The shark and fish teeth are housed in the Natural Science Museum in Bratislava. Tooth photographs were taken by JSM-6390 (JEOL) scanning electron microscope in the Banská Bystrica Department of the SAS Geological Institute and in the State Geological Institute of Dionýz Štúr in Bratislava.

Magnetic susceptibility (MS) and rock magnetic studies were performed in the Paleomagnetic Laboratory of the Polish Geological Institute–National Research Institute in Warsaw. MS was measured in 143 samples using KLY-2 kappabridge (AGICO Brno, frequency 0.92 kHz), and normalized for mass. Rock magnetic experiments on pilot collection of 22 specimens included measurements of MS in low (0.47 kHz) and high (4.7 kHz) frequency using a Bartington MS2 susceptibility meter (to evaluate the contribution of the very fine magnetic fraction close to superparamagnetic state), isothermal remanent magnetization (IRM) applied in the field of IT,

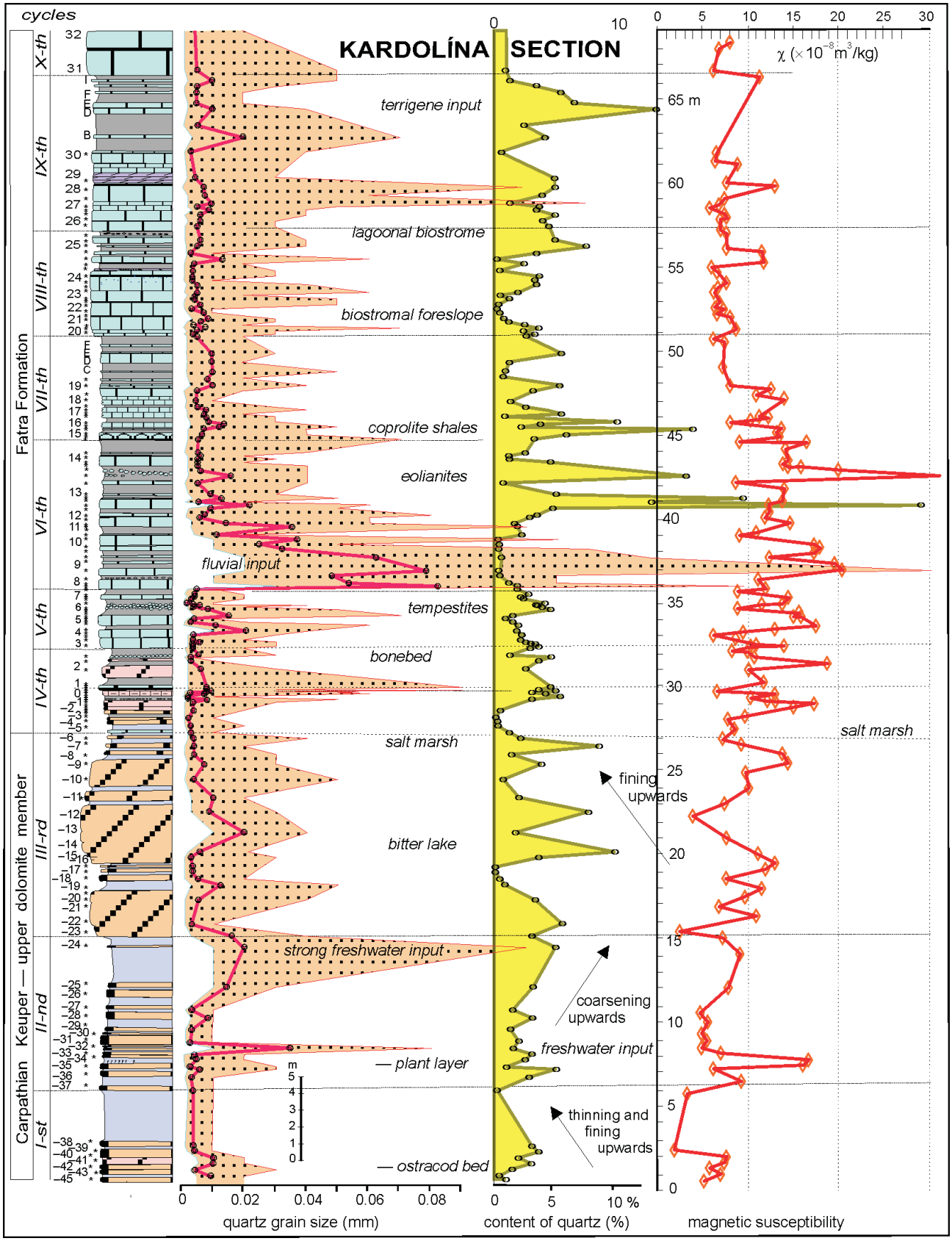

Fig. 4. Quartz grain size (left column, average size denoted by thick line) and percentage content of quartz grains (right column). Each point was obtained by averaging of 200 measurements in a particular thin section with the use of the NIS system. Right column: Magnetic susceptibility of the Kardolína section sequence and interpretation of sedimentary environment. Lithological signs same as in Fig. 5.

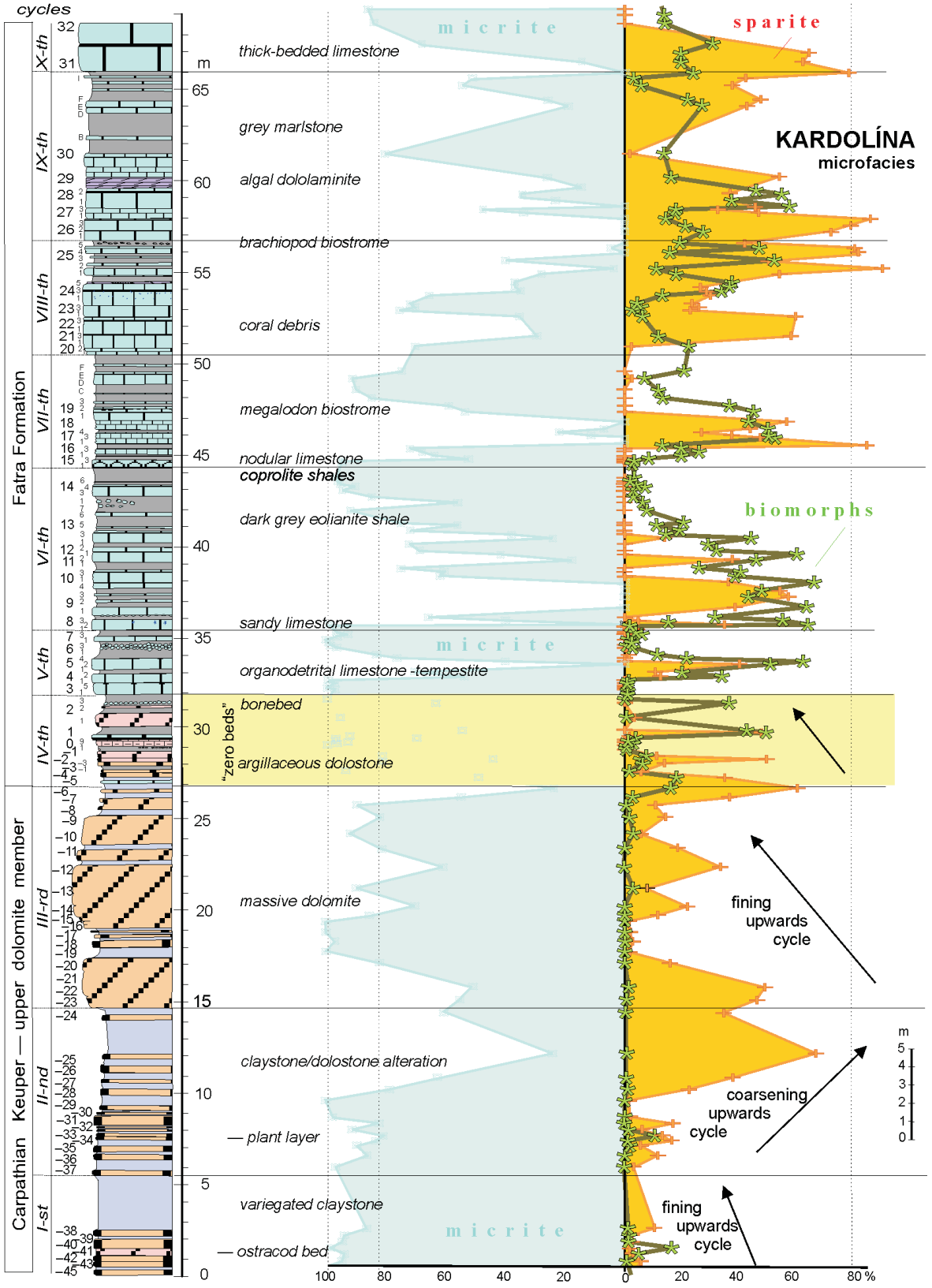

Fig. 5. Lithological composition of the uppermost three cycles of the Carpathian Keuper and the lowermost seven cycles of the Fatra Formation in the Kardolína section. Left: Lithological log shows numbering of beds in negative numbers down from the Fatra Formation base in the Carpathian Keuper, but in positive numbers upwards in the Fatra Formation proper. Micrite content (in percent) increases to the left from the zero axis, antagonistic sparite representation increases to the right. Bioclasts content indicated by asterisks: their content is positively related to sparite in the lower part of the sequence, but inversely in the upper part, indicating autochthonous occurrence of benthic organisms.

and then antiparallel in the 100 mT field, by means of MMPM1 pulse magnetizer. S-ratio, calculated as a ratio of IRM intensities applied in both fields was indicative for relative proportions of low and high coercivity minerals.

Results

Lithology and fossils

The Carpathian Keuper

Two of the three informal members recognized by Michalík (1977) in the Carpathian Keuper sequence, namely the "lower clastics" and the "main claystone" are covered below the scree (Rychliński 2008). The thirty meters thick sequence of mixed terrigenous, lacustrine, fluvial and eolian variegated greenish and violet-red dolomitic claystones with occasional intercalations of pale greenish-grey clayey dolostone, exposed in the Kardolína section, represents the uppermost part of the Carpathian Keuper ("upper dolomite member" of Michalík, l.c.). Bedding planes of rusty weathering pale greenish-grey dolomicrite layers (20 to 130 cm thick) sometimes bear ripple marks. Interbeds of yellow-, violet-, or dark grey claystone may attain thickness of 20 to 160 cm, but sometimes they are only few centimeters thick.

- "Unit I" is typical of thinning- and fining upwards architecture (65 to 20 cm). Grey biomicrite with raised $CaCO_3$ content (Beds –43 to –41) contains dispersed quartz grains (0.005 to 0.2 mm in diameter; Fig. 4) and numerous ostracod tests (3 to 10 %; Fig. 5). Higher up (in Beds –40 to –38) the dolomicrosparite content increases (to 9 %), and fragments of plants become abundant. Dolostone layers are followed by a 330 cm thick brown claystone interval.
- Dolomicrite layers (14 to 65 cm thick) of the "unit II" of lumpy texture contain dispersed tiny dolomite crystal nuclei becoming abundant upwards, where dolomicrosparite and even dolosparite prevails. Claystone interbeds are 2 to 60 cm thick. Grey claystone lense in basal part (interbed between Beds –35 and –34) contains rich and relatively large carbonized fragments of plants.
- "Unit III" forms an eminent rock step of thick (20 to 130 cm) dolostone layers. Dolomicrosparite on the base (Bed –23) contains small plant fragments. Dolomicrite beds (Beds –22 to –16) are of lumpy structure, with an admixture of eolian quartz silt (0.02 mm), larger quartz grains (0.04 to 0.05 mm) are rare, tiny plant fragments occur occasionally. Dolomicrosparite beds (Beds –15 to –11) contain sparry crystallites, dolomicrite occurs in irregular nests and lumps. Lumps, pellets, phytoclasts and tiny shell fragments occur in dolomicrite in the upper part (Beds –10 to –6). Biodetritus (ostracods, foraminifers, bivalve shell fragments, fish teeth and scales) become frequent in the uppermost layers (Beds –7 and –6).

The Fatra Formation

The Fatra Formation attains a thickness of 96 m here, in contrast to other places where it does not exceed 25 to 53 meters. Michalík (1978), Michalík et al. (1979), Gaździcki et al. (1979) divided the sequence into two biostromal members, separated from each other by a "barren interval", from the underlying Carpathian Keuper by "basal beds", and from the overlying Kopieniec Formation by "transitional beds". However, detailed study of the Kardolína section shows that the architecture of the Fatra Formation is much more complex.

- Transgressional "unit IV" (Figs. 4–5): Each of five palustrine (shallowing upwards) cycles (Beds –5 to 2.3; Fig. 5) starts with grey dolostone or even with dark organodetrital limestone and intercalation of dark brown to black-grey shale. The sequence was reduced by condensation and resedimentation (pale dolostone clasts dispersed in clayey matrix, dark crusts, erosion on bed surfaces).

Dark to black-grey argillites (70–120 cm thick) contain small pieces of carbonized wood, ooids, bone fragments, shark teeth, linguloid brachiopods, bivalves and black interlayers of laminated bituminous argillitic lime dolostone. Wavy (flaser) and parallel lamination appears in dolostone intercalations in the middle of black shales. Black ferruginous/phosphate crusts enriched by dispersed tiny rock clasts, fish teeth and bone fragments occur on upper bedding planes.

Fine clastic laminae in Beds –4, –3 and in the "zero beds" (0.1 to 0.8) contain numerous foraminiferal tests (*Agathammina austroalpina* Kristan-Tollmann & Tollmann; Figs. 4 and 6a–b; 15 to 60 in one thin section), indicating deposition in a low-energy environment, most likely on tidal flats.

U-shaped spreiten-burrows (with diameter of 35 to 40 mm) of *Rhizocorallium jenense* Zenker, parallel or oblique to bedding plane occur on the base of the dark marlstones of Bed 0.2 (Fig. 6c). Their limbs are more-or-less parallel. The tube ornamented by scratchy bioglyphes is 5 mm wide, its length is greater than 150 mm. Spreite lamellae of coarser sediment with rounded litho- and bioclasts (1 to 2 mm) usually attain diameters of >1:5.

The oldest bivalve molluscs (*Modiolus minutus* Lamarck) appear in the Bed –3.2. Higher levels of the "zero beds" (0.3 and 0.4) contain more diverse bivalve fauna: *Bakevellia praecursor* (Quenstedt), *Isocyprina ewaldi* (Bornemann), *Modiolus minutus*, *Neoschizodus*? sp., *Pleuromya*? sp.

The yellowish weathering fine-organodetrital limestone layer (Bed 1) contains a lot of broken shells correlatable with water turbulence, rather than with micrite content. Clastic quartz grains are rare and rather small, bearing signs of wind- not of riverine transport. Biodetrital limestone is followed by brown claystone intercalated by dolostone layers with bone-bed type surfaces. Condensation occurs near the top of individual layers, sometimes connected with enrichment of phosphatic matter, fine breccia and teeth and bone fragments ("bonebeds" 2.1 and 2.2; Fig. 7).

A shark tooth of *Hybodus minor* Agassiz and another 23 teeth belonging to *Lissodus minimus* Agassiz were collected in Beds 0.4 and 2.1. The symmetrical tooth of the first species is 1.5 mm high. High, upright central cusp flanked by up to four pairs of lateral cusplets with fairly wide base is lingually inclined in lateral view. Fairly coarse vertical ridges descend cusps from apices, occasionally bifurcate basally. Lateral cutting edges of cusps are sharp. Shallow root lingually projects in so-called "lingual torus", roughly semicircular in basal

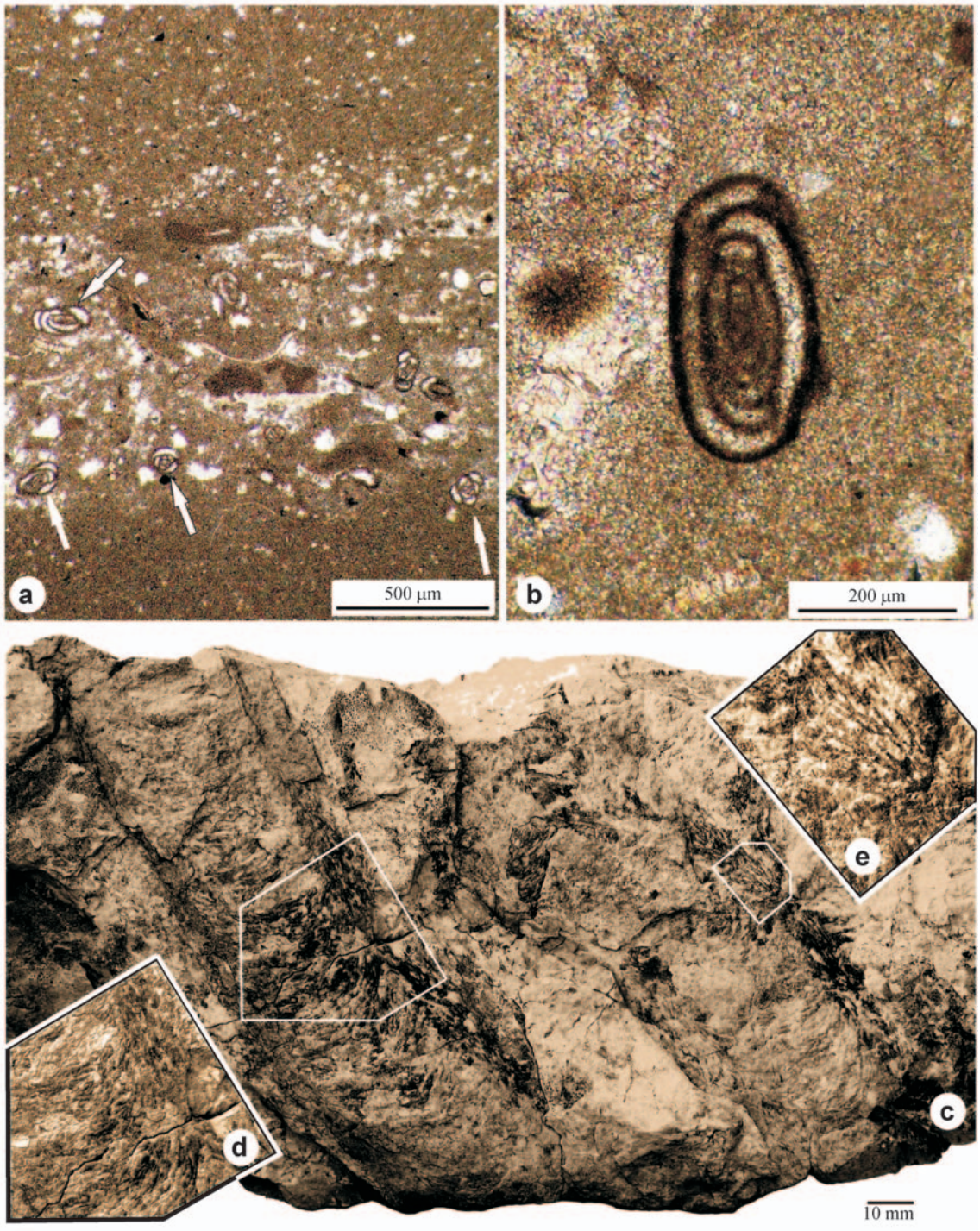

Fig. 6. a — Foraminifer *Agathammina* microfacies (the best preserved specimens are arrowed), Kardolína section, Fatra Formation base (Bed 0.3). **b** — *Agathammina austroalpina* Kristan-Tollmann & Tollmann, 1964, layer 0.4. **c** — *Rhizocorallium jenense*, Bed 0.2. **d** — spreite lamellae bordered with U-tube. **e** —scratches inside the U-tube.

view and perforated by numerous vascular foramina. Labial face attains less than one-fifth of total tooth height.

Teeth of *Lissodus minimus* are up to 4 mm long. Low crown with stubby central cusp is flanked by up to five pairs of very low lateral cusplets and ornamented by series of often bifurcating vertical ridges descending from cusp apices on labial and lingual faces. Longitudinal ridge surrounds tooth along surface of crown shoulder. Lateral margins of crown extend well beyond crown/root junction. Distinctive peg-like expansion of central cusp is situated low down on labial side. Pressure scar resulting from tooth to tooth contact in the jaw often developed in corresponding position on lingual side of central cusp. Root is of approximately same height as crown and projects slightly lingually from crown undersurface. Its upper face on labial side

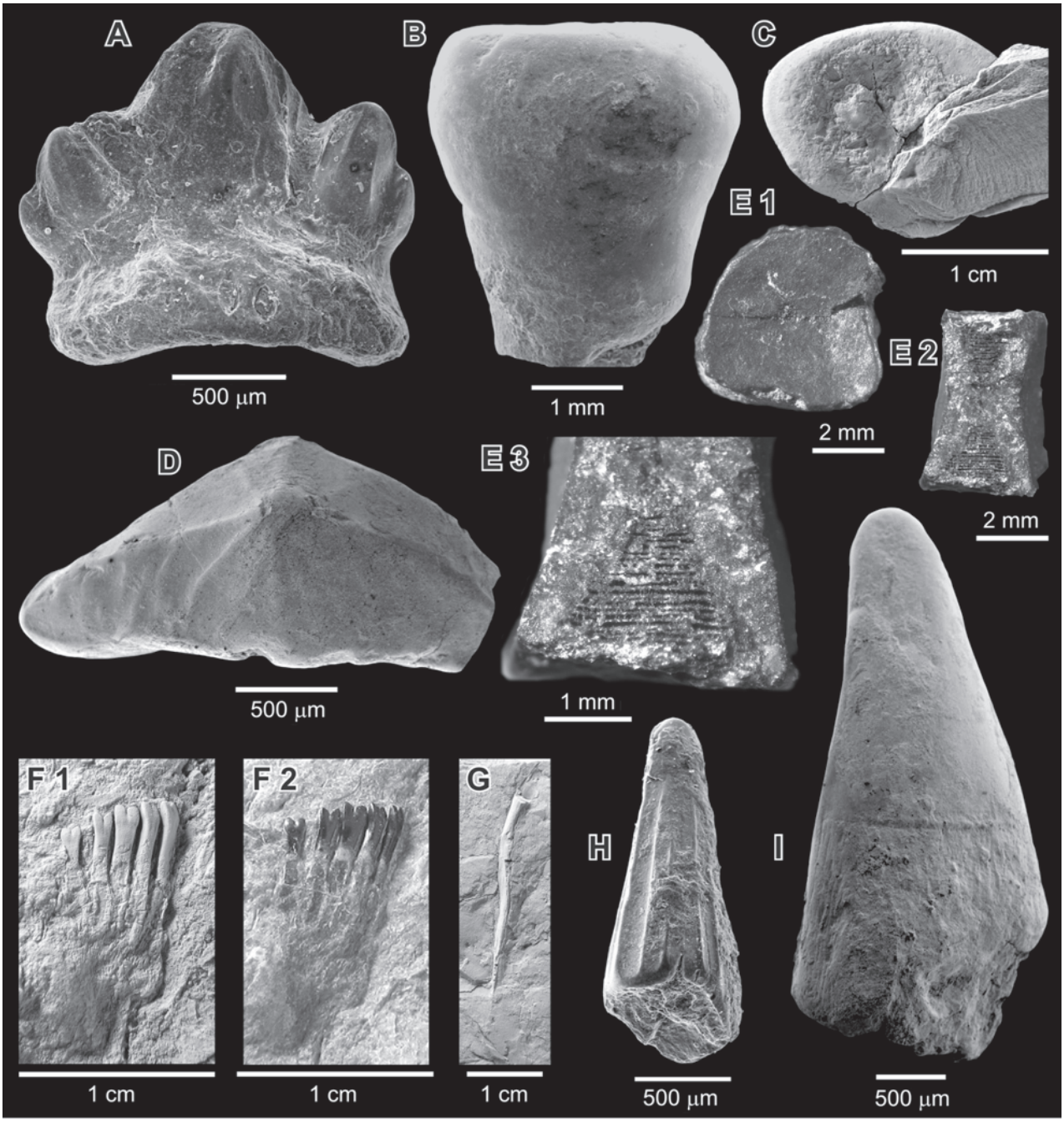

Fig. 7. Shark and fish teeth and vertebrae from bonebeds in transitional cycles of the Fatra Formation in the Kardolína section. **A** — *Hybodus minor* Agassiz, 1837; **B** — molariform tooth of *Sargodon tomicus* Plieninger, 1847; **C** — fish vertebra; **D** — *Lissodus minimus* Agassiz, 1839; **E** — fish vertebra; **F1, 2** — incisiform tooth of *Sargodon tomicus* Plieninger, 1847; **G** — vertebral spine?; **H, I** — *Severnichthys acuminatus* (Agassiz, 1835), H — tooth of "*Saurichthys longidens*" type; I — tooth of "*Birgeria acuminata*" type.

Fig. 8. Rhaetian bivalves from basal part of the Fatra Formation, Kardolína section. White scale bars = 1 cm. **A, B** — *Placunopsis*? *alpina* (Winkler, 1859). Two left valves with xenomorphic sculpture. Specimen on the left side was originally attached to the closed ventral margin of another, probably "pectinid" species, Bed 8; **B** — Left valve (coll. 5.1/94), Bed 5.1v; **C** — *Bakevellia praecursor* (Quenstedt, 1856). Internal mould of right valve, Bed 2.3; **D, G** — *Rhaetavicula contorta* (Portlock, 1843), D — right valve, G — left valve, Bed 2.3; **E** — *Palaeocardita austriaca* (von Hauer, 1853), right valve, Bed 8; **F** — *Gervillaria inflata* (Schafhäutl, 1851), right valve, Bed 5.1 (coll. 5.1/72); **H** — *Elegantinia emmrichi* (Winkler, 1859), right valve, Bed 5.1 (coll. No. 5.1/61); **I, J** — *Entolium* (*Entolium*) aff. *lunare* (Roemer, 1839), I — External mould of the dorsal part of right valve. Byssal notch is developed below the anterior auricle, J — left valve, 10; **K** — *Propeamussium* (*Parvamussium*) *schafhaeutli* (Winkler, 1859), left valve. Impressions of internal radial ribs are visible in the central part of the discus, Bed 10;

Continued on the next page

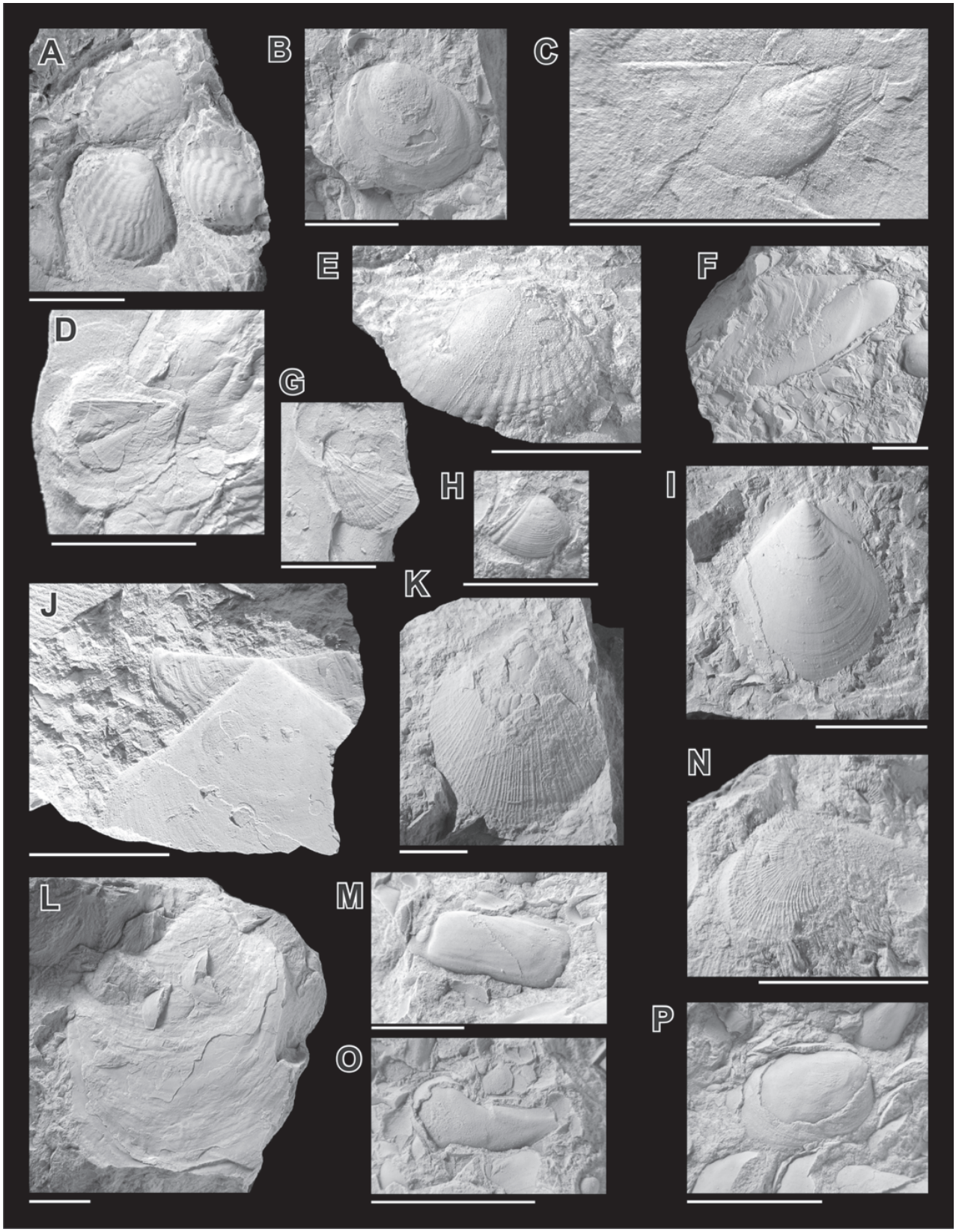

Continued from the previous page

L — *Plicatula archiaci* (Stoppani, 1861), left valve, Bed 5.1v (coll. 5.1/94); **M** — "*Permophorus*" *elongatus* (Moore, 1861). Internal mould of the left valve, Bed 5.1v; **N** — *Atreta* "*intusstriata*". Right valve cemented on the surface in the umbonal part of the *Propeamussium* (*Parvamussium*) *schafhaeutli* (Winkler, 1859), left valve, Bed 10; **O** — *Nuculana* (*Nuculana*) *deffneri* (Oppel, 1856), left valve, Bed 5.1 (coll. 5.1/3); **P** — *Botulopis faba* (Winkler, 1859), right valve, Bed 5.1.

is very shallow, bearing a longitudinal row of tiny vascular foramina. Labial face of root is concave, containing much larger, randomly distributed foramina in its lower portion.

Fish are represented by four molariform and incisiform teeth of *Sargodon tomicus* Plieninger (Fig. 7) and conical teeth of *Severnichthys acuminatus* (Agassiz), a "primitive" basal actinopterygians. Two tooth types are recognized within the latter species, each of which has previously been assigned to a separate taxon: "*Birgeria acuminatus*" type (4 teeth) and "*Saurichthys longidens*" type (2 teeth).

• Tempestite "unit V". This four and half meters thick limestone sequence (Beds 3–7) consists of bedded (10–30 cm) grey biomicrites to calcarenites with wavy bedding planes. They contain frequent mollusc and brachiopod shells, sometimes with distorted geopetal fillings. Loadcasts and erosional marks on the layer bases, and gradation of clasts occur frequently, indicating origin in distal tempestite lobes laid on a soft marly bottom. Intensive storm activity seems to be a typical feature of the environment during sedimentation of this cycle.

Between loadcasts, deformed tubular bodies with typical Y-shaped structure and ramification attributable to *Thalassinoides* sp. occur. These traces were produced by crustaceans (Bromley 1996) indicating omission surfaces due to sudden erosive events (Mikuláš 2006).

Foraminiferal diversity increases upwards (*Aulotortus friedli*, *Aulotortus*, *Frondicularia*, *Planinvoluta*, *Ophthalmidium*, *Nodosaria*). They are accompanied by other marine organisms (*Aciculella*, *Theelia*, solenoporaceans, ostracods). The first brachiopods appear in Bed 5.4.

The preservation of originally aragonite shells (recrystallized or as internal or composite moulds) of four bivalve associations recognized within this cycle proves that the fossil record was not depleted and it represents the original composition.

a. The *Rhaetavicula contorta* association (Bed 2.3; Figs. 8, 9, 11c) characterized by dominance of epifaunal byssate- (46 %), semi-infaunal byssate- (30 %) and cementing bivalve types (18 %) is composed of suspension feeders. Pectenids like *Propeamussium* (*Parvamussium*) *schafhaeutli* (Stur) and *Chlamys mayeri* (Winkler) were present among these first bivalve colonizers. Right valves of *Rhaetavicula contorta* (Portlock) occur rarely (Fig. 8; similarly to statements of Pflücker & Rico 1868; Cox 1961; Ivimey-Cook et al. 1999). Relatively small shell size and lack of infaunal molluscs points to nutrient-poor and dysoxic substrate, their preservation (left and right valves together, no fragmentation but post-mortem disarticulation only) indicates low water energy above a soft but stable substrate. A possible epifaunal character of these animals attached to sea plants can be considered, too.

The mixed *Rhaetavicula contorta* and "*Placunopsis*" *alpina* association (Bed 4; Fig. 8; 34 % of byssate epifauna, 25 % of byssate semi-infauna) reflects diversification within a quiet, nutrient poor environment on a firm and stable substrate in a carbonate regime. Increase of cementing bivalves ("*Placunopsis*" *alpina:* up to 30 %) could have been associated with a firmer substrate (abundant bioclasts, shell fragments).

b. The tempestite coquina of 5.1 Bed contains accumulations of large dissarticulated convex down (both right and left) *Gervillaria inflata* (Schafhäutl) and "*Permophorus*" *elongates* (Moore) valves with soft body imprints (Figs. 8–10, 11b). The association is composed of byssate semi-infauna (50 %), shallow infauna, mobile- (34 %), or byssate epifauna (14 %), which, with the exception of one detritus eater (*Nuculana* sp.), were suspension feeders. This fact indicates a firm and stable substrate in a high energy environment, supplied with food in suspension. Despite reworking and mixing, right and left valve ratio does not indicate any significant sorting (Fig. 9). Shell accumulation of the "*Corbula*" *alpina* association dominated by shallow infaunal suspension feeders (93 %) occur at the base of Bed 7b (Figs. 9, 10). The composition of this storm shell accumulation is identical to that of soft-bottom bivalve association of the underlying marlstone. Lack of epifauna could be associated with the scarcity of attachment opportunities. On the upper bedding plane of this bed, clusters of *Rhaetavicula contorta*, rarely of *Modiolus minutus* occur. Shallow infaunal suspension feeders are dominant (96 %) in the association from the Bed 9.3 (Fig. 11). This 1.5 cm thick accumulation resembles that of the Bed 7b. However, while the former association occurs on the tempestite base, the latter one is situated in the upper part of the bed as a result of erosion of fine mud by bottom currents. Convex-up and down and also articulated shells occur. The underlying marlstone contains the same species composition which indicates conditions similar to Bed 7b.

c. Sorting due to storm activity formed temporary firm substrate for cementing larvae of "*Placunopsis*" *alpina*, of large *Plicatula* sp. and of attached *Atreta intusstriata* forming shell accumulation (Figs. 8–11a). Epifaunal cementing bivalves are dominant (65 %) in this association (Beds 5.1v, and 8b; Fig. 9), followed by epifaunal byssate (30 %) and semi-infaunal byssate bivalves (10 %). In spite of some redeposition, bivalve composition indicates a firm and stable substrate. The "*Placunopsis*" *alpina* shells are exclusively left upper valves. While Triassic "*Placunopsis*" shells cemented to the substrate (Seilacher 1954; Hölder 1990; Hautmann 2001), Jurassic forms attributed to different taxa were byssus-attached (Todd & Palmer 2002). Secondary texture patterns (Fig. 8a,b) developed on left valves copying the surface of the substrate of their right valves. However, the texture resembles radially ribbed bivalves, which are not common in the association (although *Paleocardita austriaca* could be one possible candidate).

d. The *Propeamussium* (*Parvamussium*) *schafhaeutli* and *Entolium* sp. association (Bed 10; Fig. 9) is dominated (42 %) by epifaunal byssate pectinid bivalves (*Entolium* sp. and *Chlamys mayeri*). Epifaunal free-lying/vagile morphotype is represented by radially ornamented left valves of *Propeamussium* (*Parvamussium*) *schafhaeutli* (32 %) only. No right (smooth and thin-shelled) valves were found, although both equally smooth and thin valves of *Entolium* sp. are common. Microstructure of both species shows aragonite shell mineralogy. Long exposure before their burial could be indicated by common cementing of *Atreta richthofeni* on both outer and inner surfaces. Hence, less resistant right valves were broken and dissolved. The association lived on a stable detrital substrate with medium water energy near the maximum storm wave base. Protected shelters under empty bivalve shells were often inhabited by ostracod populations (Fig. 12).

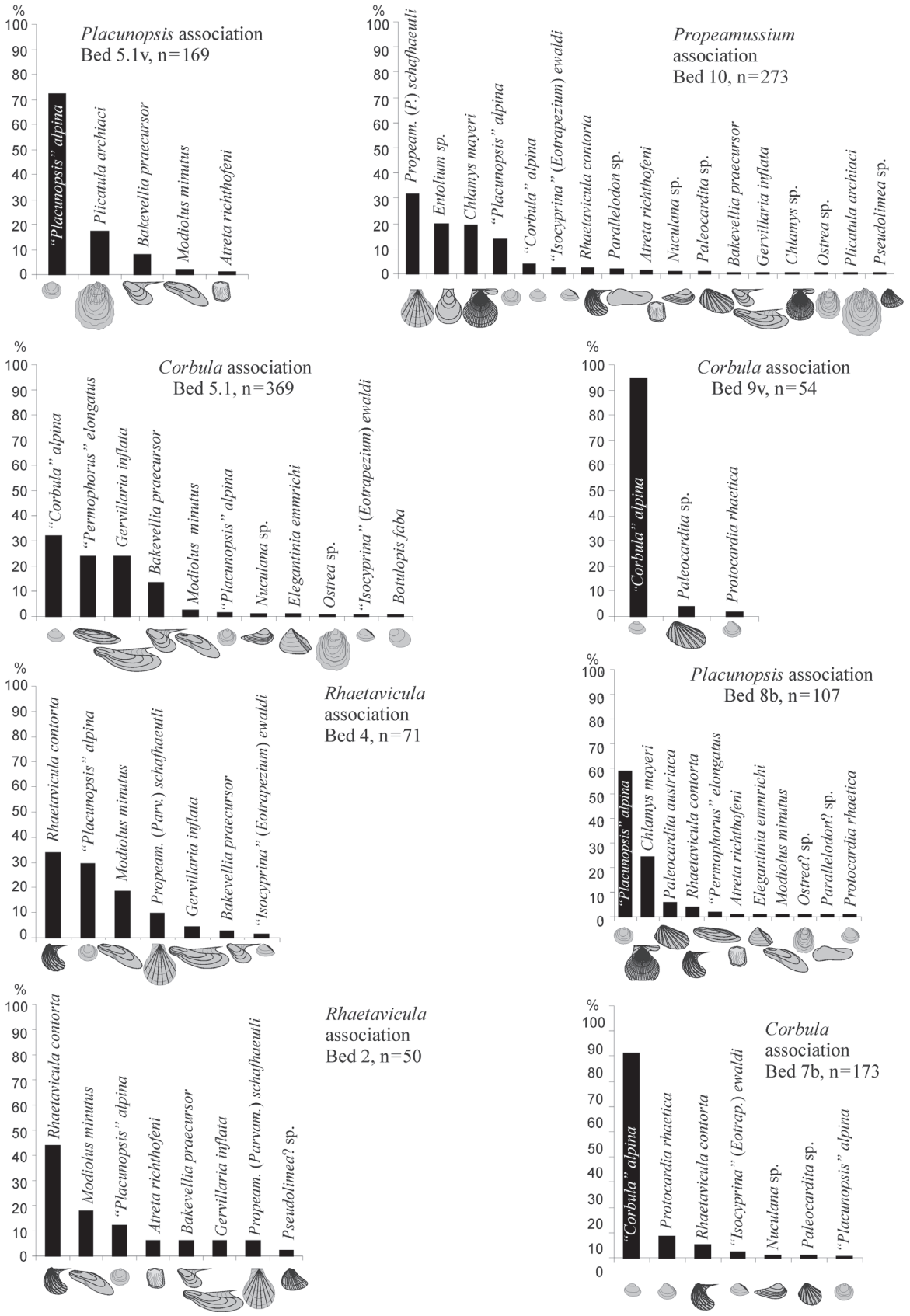

Fig. 9. Histograms showing percentual representation of species in bivalve assemblages from individual beds in basal part of the Fatra Formation, Kardolína section.

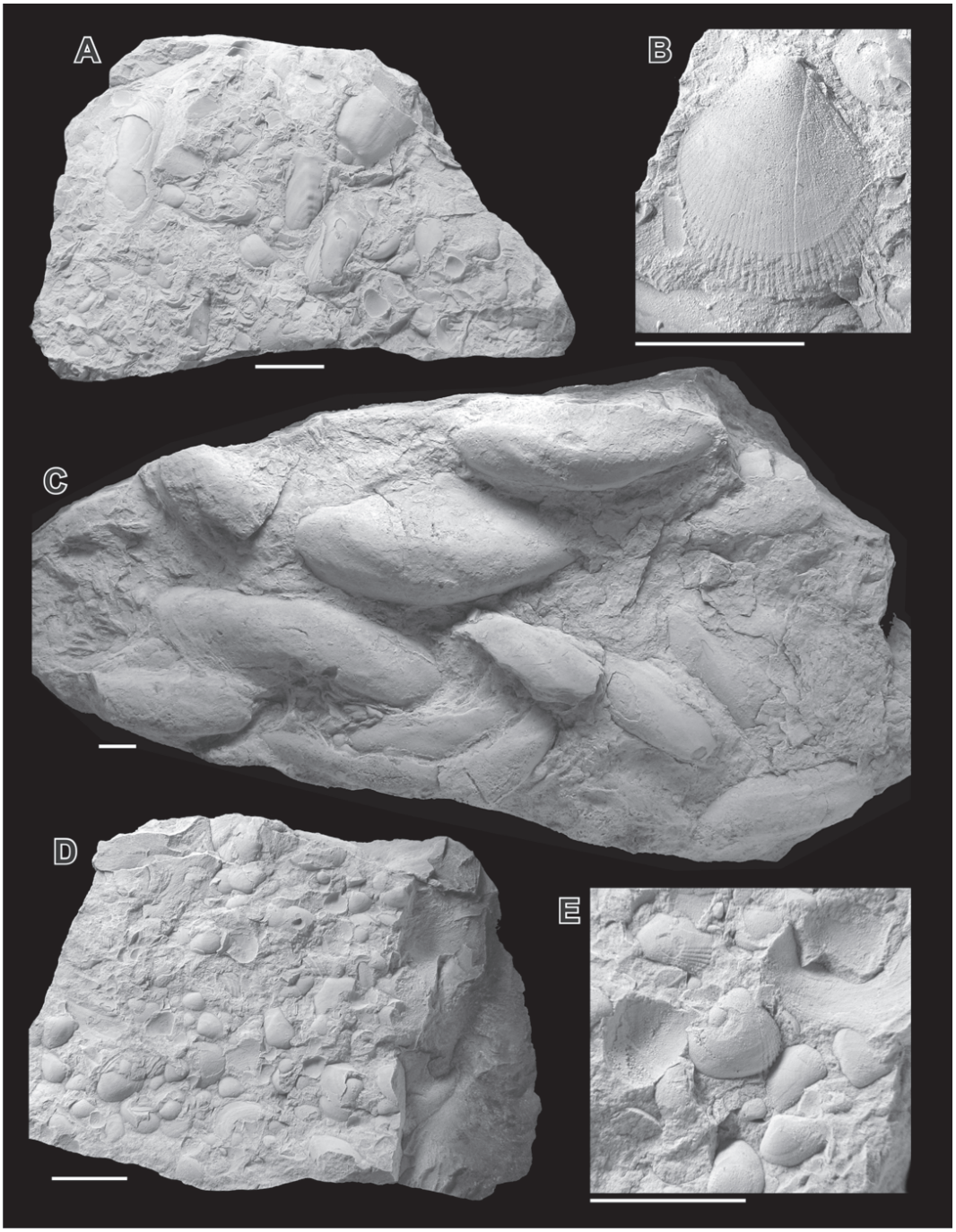

Fig. 10. Rhaetian bivalves from basal part of the Fatra Formation, Kardolína section. White scale bars = 1 cm. **A** — "*Permophorus*" *elongatus* (Moore, 1861). Storm accumulation of shells, Bed 5.1 (coll. No. 5.1/2); **B** — "*Chlamys*" *mayeri* (Winkler, 1861), left valve, Bed 8; **C** — *Gervillaria inflata* (Schafhäutl, 1851). Stormy shell accumulation on the lower bedding plane, Bed 5.1; **D** — *Corbula alpina* Winkler, 1859. Shell accumulation on the lower bedding plane, Bed 7; **E** — *Protocardia rhaetica* (Merian, 1853). Moulds of the right (upper left corner of photo) and left valves (in the middle of the photo), Bed 7.

• "Unit VI" — eolianites. Thick limestone layers (Beds 8 and 9) form the base of the sixth, 12 m thick unit. It is formed by dark brown aleuritic marl with intercalations of dark grey fine detrital argillaceous limestone (fining and thinning upwards cycle). Abundant quartz grains attaining diameters of 0.02 to 0.03 mm indicate eolian transport. Burrows of infaunal organisms occur in the uppermost parts of the layers.

Two types of isolated fish teeth from Beds 13/14 and 14 belong to *Sargodon tomicus* Plieninger, 1847. The molariform type is characterized by a hemispherical crown up to 4 mm in diameter, circular to oval in occlusal view, often heavily worn. Wearing reveals characteristic pattern of underlying dentine, consisting of radial network of large cavities with finely branching canaliculi at their ends. Molariform teeth were

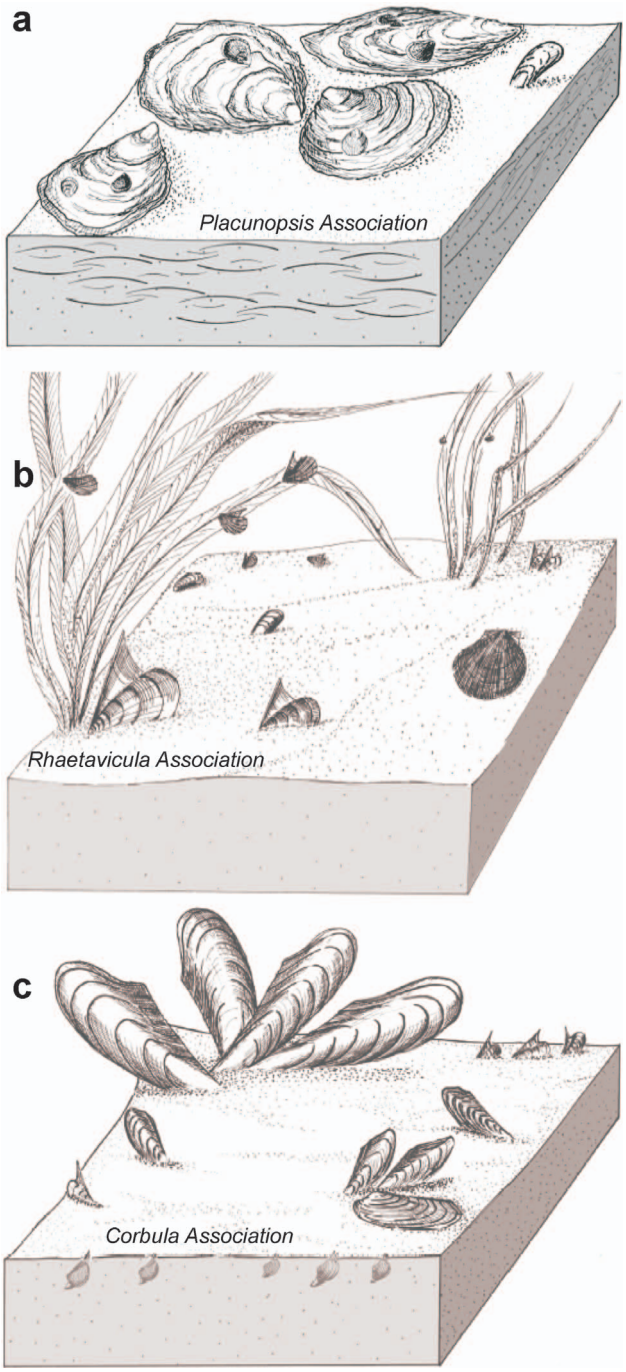

Fig. 11. Graphic reconstructions of three Rhaetian bivalve assemblages from the lowermost part of the Fatra Formation, Kardolína section. **a** — "*Placunopsis*" *alpina* assemblage, Bed 5.1v; **b** — *Rhaetavicula contorta* assemblage, Beds 2.3 and 4; **c** — "*Corbula*" *alpina* assemblage, Bed 5.1.

Fig. 12. Valve of *Placunopsis alpina* with cluster of ostracods immediately inside. Scale bar is equal to 10 mm.

arranged in longitudinal rows on both upper and lower jaws, with the smallest teeth in front and at sides of dentitional pavement. Incisiform teeth up to 14 mm long comprise chisel-like crown surmounting a deep root. Lingual face of crown is divided into two by a wear facet in centre produced by functional ante-mortem contact abrasion. As in all bifid crowns, highest cusp is located closest to midline of mouth. Incisiform teeth were used to pluck bivalves from the substrate, and the battery of molariform teeth provided an effective mill for breaking their shells (Swift & Martill 1999). Teeth of *Birgeria acuminata* (Agassiz) were found between Beds 13 and 14.

- "Unit VII". The seventh unit is about 10 m thick; it starts with sandy organodetrital limestone (Beds 15 and 16) with nodular appearance (flaser texture). Intercalations of black marls are rich in coprolites, fish teeth, pectenids and other bivalve shells, and crinoids. Layer 19 contains large megalontid bivalve shells. Higher up, the clay content increases.
- "Unit VIII". Thick-bedded limestones (Beds 20–24) contain debris of corals transported down the submarine slope. Other organic fragments (bivalve shells, crinoids, ossicles) are less frequent. Intercalations of grey marl with brachiopods *Rhaetina gregaria* (Suess) in situ appear in the upper part of this unit.
- "Unit IX". The ninth unit starts with detrital limestone. Thick algal dololaminite layer (Bed 29) preserved fine record of dolostone rhythms. Marls increase in the higher part of the thinning upwards cycle.
- "Unit X". The tenth unit consists of thick-bedded fine organodetrital limestones of slope facies. This lithology records the start of a general deepening of the basin.

Magnetic susceptibility and rock magnetic properties

MS values are moderately high for carbonate rocks, mostly in the range between 5 and 20×10^{-8} m^3/kg, with a single maximum above 30×10^{-8} m^3/kg (Fig. 4). An increasing trend was observed from the bottom (Carpathian Keuper facies) up to the middle part of the section, with maximum values in

the lower part of the Fatra Formation, at the bottom of the VI-th cycle (Fig. 4), followed by a decreasing trend in the upper part of the Fatra Formation. All pilot samples studied revealed significant MS frequency dependence (Fig. 13a) which accounts for contribution of ultrafine magnetic particles, close to superparamagnetic to single domain state to MS (Forster et al. 1994; Grabowski et al. 2009). As there is also a very good correlation between MS and IRM intensity acquired in the 1 T field (Fig. 13b), it is necessary to conclude, that MS is based mostly on ferromagnetic minerals. Magnetite seems to be the most important magnetic, as inferred from predominantly low coercivities — samples are almost saturated in the field of 300 mT (Fig. 13c) and maximum unblocking temperatures of low and medium coercivity fraction (0.1 T and 0.4 T respectively; Fig. 13d) between 500 and 550 °C. Subordinate amounts of hematite occur as well, as is indicated by slightly increasing IRM intensity above 500 mT (Fig. 13c), and maximum unblocking temperatures around 650 °C for the high coercivity (1.4 T) fraction (Fig. 13d).

Geochemistry

Major elements

Total rock analyses of 12 samples were performed (Table 1) in order to obtain a more precise idea of the origin of the source material and to determine chemical changes potentially forced by hydrological, climatic and other factors. The chemical composition of the samples is given mainly by the proportion of carbonate (represented by CaO, MgO) and silicates (represented by SiO_2, Al_2O_3; Table 1). The dolomite non-carbonate content is higher (approximately 20 to 30 %) than in limestones (approximately 5 to 15 %; Fig. 16). Samples –34, –3.2 and 14 can be designated as argillites, as their carbonate content is low (< 5 to about 30 %; Fig. 6).

The composition of major elements in argillites is close to the Post-Archean Australian Shale (PAAS) composition and could indicate that (weathered) felsic rocks were the probable source of our sediments (German et al. 1991; Condie 1993; Bau & Dulski 1996). These characteristics are in line with the mineral composition of samples analysed. Illite with only very low content of smectite dominates in the clay size fraction of samples 32, –3.2, 14, 19G. The clay composition of samples both from the Carpathian Keuper or from the Fatra Formation is almost identical (Biroň in the Środoń et al. 2006, or in Michalík et al. 2010).

In spite of relatively low values, P_2O_5, MnO, and S_{tot} contents are higher in the Fatra Formation limestone than in the Carpathian Keuper dolostone: they document a shift in sedimentary and diagenetic conditions associated with marine transgression. P_2O_5 enrichment was probably related to increased bioproductivity in the marine basin indicated by bonebed occurrence.

Trace elements and REE

Low silicate admixture complicates the interpretation of large ion lithophile elements (LILE: Rb, Cs, Ba), with the exception of Sr. The LILE substituting K are accumulated in the phyllosilicates in both parts of the sequence. High Sr content in carbonate (495–861 ppm) in comparison with the argillites (135–228 ppm) and high correlation of Sr vs. Ca ($r > 0.9$) documents Ca vs. Sr substitution, typical of biogenic aragonite or of a phase precipitated from evaporated marine water or brine (Rosen et al. 1989; Garcia del Cura et al. 2001; Korte et al. 2005). Carpathian Keuper dolostones are enriched in Sr but more depleted in total sulphur ($S_{tot} \approx 0.02$ %) than limestones (0.02 to 0.55 %) of the Fatra Formation (Table 1). In accordance with the facies scheme presented, it is possible that dolomite comes from the sulphate-free fluvial/lacustrine waters (Warren 2000; Garcia del Cura et al. 2001 and their references). However, low S content could result from diagenetic leaching of sulphate. By analogy, higher S_{tot} content and pyrite grains observed in thin sections of limestone document a marine-water environment. Framboidal aggregates represent a typical diagenetic pattern of pyrite: they indicate more O-depleted diagenetic conditions than those of limestone accumulation. Low C_{org} content was connected with balanced productivity and, locally, with higher input of terrestrial organic debris, as indicated by the quality of the organic matter and by C-isotope analyses.

The compositional pattern between the incompatible elements Th and Y and the compatible Sc, Cr, V and Ni indicates that the sediment is more likely to have originated from a felsic than from a mafic source (Fig. 14; Table 1). Incompatibility of Th and Y results in their higher concentration in well differentiated felsic rocks (Condie 1993; Cullers 2000). The Th/Sc ratios are generally similar to the ratio reported for the PAAS (0.91). The Y/Ni ratios of sediment studied are higher than these of the PAAS (0.49). In spite of high Cr/Th and Cr/V ratios (PAAS = 7.53; 0.73 respectively), the samples are closer to the felsic source and point to local enrichment of Cr-minerals rather than to origin from a mafic source. This conclusion fits with the interpretation of major elements and with mineral composition.

The total rare earth elements (TREE) contents in the argillite samples are similar to those of PAAS (Condie 1993; Cullers 2000). The samples –32 and 14 display flat PAAS-normalized REE pattern with little depletion of heavy REE (HREE; Fig. 15). The sample –3.2 (IV-th cycle) reveals weak HREE enrichment expressed by ratios $Gd_N/Yb_N = 0.8$ and $La_N/Yb_N = 0.69$. All three samples show weak negative Eu anomaly (Eu/Eu* = 0.82, 0.77 and 0.94; Table 1) whereas Ce/Ce* ratios are close to unity and record very weak negative Ce anomaly.

Dolostones of the Carpathian Keuper are depleted of REE relative to PAAS (0.2 to 0.4) and show slight positive Eu anomaly (Fig. 15; Table 1). Fatra Formation limestones are depleted relatively to PAAS but the elements from Sm to Ho (middle — MREE; Ounis et al. 2008) relatively increased to 0.5–0.6 content of PAAS. The Eu values reach PAAS level and show positive Eu anomaly. Increased content of the MREE documents different fractionation of REE in the Fatra Formation limestones in comparison with the Carpathian Keuper dolostones and can be interpreted in line with sedimentary evolution.

C and O isotopes

The results of C-isotopic analyses indicate two individual terrestrial vs. marine sources of organic matter. Less negative

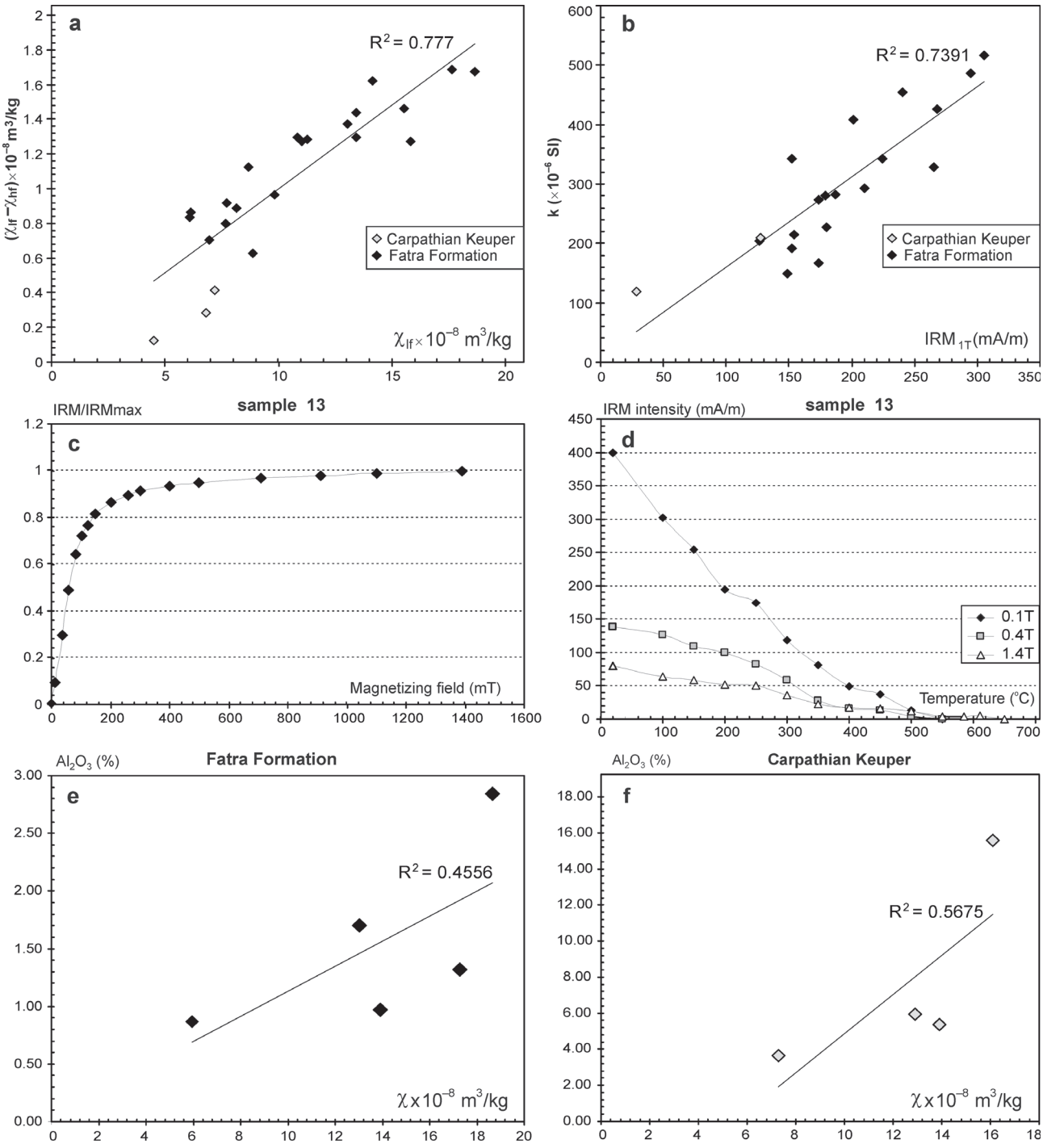

Fig. 13. Rock magnetism and its correlation with geochemistry: **a** — Diagram of frequency dependence of magnetic susceptibility: difference between low frequency MS (χ_{lf}) and high frequency MS (χ_{hf}) plotted as a function of χ_{lf}. **b** — Correlation between volume magnetic susceptibility (k) and intensity of isothermal remanent magnetization acquired in the field of 1 T ($IRM_{1\,T}$). **c** — Stepwise acquisition of IRM, sample 13. **d** — Thermal demagnetization of 3 axes IRM acquired in the fields of 0.1 T, 0.4 T and 1.4 T. **e** — Correlation between mass normalized MS (χ) and Al_2O_3 content, Fatra Formation. **f** — Correlation between mass normalized MS (χ) and Al_2O_3 content, Carpathian Keuper.

values (–24.63 to –24.45 ‰ VPBD) occur in Beds –34/1, –34/2 and 19G, 19F with higher content of plant debris, in contrast with more negative ones (–27.27 to –25.64 ‰ VPDB) coming from the Beds –5 to +13 containing organic matter with more marine character (Fig. 16, see palm tree marks).

The C and O isotope data demonstrated in plots (Figs. 16, 17) document different character of two carbonate production systems represented by Carpathian Keuper dolostones and Fatra Formation limestones in the Kardolína section. The values of both carbon and oxygen isotopic ratios achieved relatively

Table 1

Element	Unit	Beds											
		25.1	19.1	14	10.3	5.5	2.3A	0.8	–3.2	–22	–15	–23	–34
SiO_2	%	3.43	5.51	53.35	8.61	9.19	11.90	6.60	56.1	17.07	14.47	20.90	62.54
Al_2O_3	%	0.87	0.97	13.30	1.32	2.26	2.84	1.70	16.67	5.36	5.95	3.63	15.58
Fe_2O_3	%	1.12	1.97	4.92	2.07	2.34	2.70	0.45	4.72	2.05	2.05	2.71	1.80
MgO	%	1.42	1.63	1.98	1.05	1.66	1.52	1.30	1.97	9.37	14.34	16.09	3.07
CaO	%	51.02	49.39	9.44	47.76	45.42	43.51	48.39	4.01	28.26	23.22	21.51	2.28
Na_2O	%	0.07	0.11	0.7	0.17	0.15	0.06	0.4	0.18	0.12	0.18	0.06	0.43
K_2O	%	0.1	0.14	2.41	0.15	0.39	0.31	0.22	4.10	1.35	1.81	0.23	4.37
TiO_2	%	0.04	0.04	0.74	0.07	0.12	0.11	0.07	0.94	0.27	0.23	0.13	1.01
P_2O_5	%	0.01	0.08	0.06	0.19	0.11	0.08	0.02	0.12	0.02	0.04	0.03	0.12
MnO	%	0.04	0.08	0.04	0.14	0.09	0.17	0.05	0.08	0.05	0.05	0.08	0.02
S_{tot}	%	0.21	0.55	0.02	0.41	0.30	0.13	0.03	0.02	0.02	0.07	0.02	0.00
LOI	%	41.8	40	12.9	38.4	37.7	36.7	40.7	10.9	35.8	37.3	34.3	8.60
Ba	ppm	8	13	165	15	28	52	20	259	214	108	45	218
Co	ppm	0.8	3.5	9.5	2.7	4.2	2.0	<0.2	38.8	2.6	3.7	5.9	6.4
Cs	ppm	0.2	0.4	7.3	0.3	0.9	0.7	0.4	8.5	2.4	3.5	0.4	7.2
Cr	ppm	< d.l.	< d.l.	108.8	< d.l.	95.2	13.6	20.4	142.8	40.8	40.8	27.2	122.4
Hf	ppm	0.2	0.3	8.3	0.4	1.0	0.4	0.3	9.6	1.3	1.1	0.7	9.5
Nb	ppm	0.7	0.9	15.9	1.4	2.4	2.1	1.6	22.3	5.6	4.7	2.5	20.7
Ni	ppm	5.4	9.5	26.9	7.1	9.5	9.4	1.5	106.4	11.9	12.1	32.7	14.7
Rb	ppm	3.8	5.7	109.1	5.7	15.5	12.7	7.3	180.8	57.2	77.5	9.4	174
Sc	ppm	0.9	2	12	2	3	3	2	16	6	6	3	15
Sr	ppm	711	530	229	689	532	494	582	119	861	430	547	136
Th	ppm	0.6	2.1	12.1	1.6	2.4	2.2	1.1	17.7	4.3	3.9	2.3	18.4
U	ppm	1.3	0.7	2.5	1.7	1.4	0.9	3.2	12	1	1.5	1.4	9
V	ppm	11	16	111	22	21	23	17	127	33	41	25	104
Zr	ppm	6.9	13.8	298.9	15.9	34	16.2	11.1	354.1	51.8	36.3	23.3	320.1
Y	ppm	3.8	11.6	27.4	11	13.9	14.9	5.2	24.5	10.7	9.7	5.3	25.3
TREE	ppm	23.36	61.72	190.65	61.12	88.73	71.78	24.84	155.21	67.88	56.09	35.42	211.64
La	ppm	4.7	12.1	39.2	11.4	17.1	13.3	5.0	29.9	12.6	10.8	6.9	38.7
Ce	ppm	9.7	22.9	81.5	24.0	33.4	26.5	9.8	64.4	28.7	22.8	14.7	91.5
Pr	ppm	1.15	3.07	9.15	3.06	4.47	3.37	1.22	7.67	3.38	2.73	1.75	10.91
Nd	ppm	4.6	13.3	35.1	13.4	20.0	15.4	4.8	29.5	13.2	10.8	7.0	43.1
Sm	ppm	0.78	2.53	6.00	2.35	3.76	3.49	0.93	5.21	2.52	2.09	1.25	7.57
Eu	ppm	0.26	0.62	1.11	0.84	1.18	0.90	0.23	0.79	0.56	0.46	0.28	1.15
Gd	ppm	0.75	2.49	5.00	2.26	3.54	3.24	0.92	4.29	2.24	1.88	1.12	5.66
Tb	ppm	0.12	0.38	0.85	0.33	0.47	0.47	0.15	0.77	0.34	0.31	0.17	0.88
Dy	ppm	0.61	2.04	4.89	1.57	2.31	2.28	0.79	4.61	1.78	1.68	0.95	4.66
Ho	ppm	0.11	0.37	1.04	0.30	0.41	0.43	0.15	0.99	0.37	0.34	0.18	0.96
Er	ppm	0.29	0.92	3.06	0.83	0.98	1.17	0.4	2.92	1.00	1.02	0.51	2.80
Tm	ppm	0.04	0.13	0.46	0.10	0.14	0.16	0.06	0.48	0.15	0.15	0.08	0.45
Yb	ppm	0.22	0.77	2.85	0.59	0.85	0.94	0.34	3.2	0.9	0.89	0.46	2.85
Lu	ppm	0.03	0.10	0.44	0.09	0.12	0.13	0.05	0.48	0.14	0.14	0.07	0.45
LaN/YbN		1.57	1.15	1.01	1.43	1.48	1.04	1.08	0.68	1.03	0.89	1.10	1.00
Gd N/YbN		2.03	1.93	1.05	2.28	2.48	2.05	1.61	0.80	1.48	1.26	1.45	1.18
EuN/EuN*		1.58	1.15	0.94	1.67	1.51	1.25	1.16	0.78	1.10	1.08	1.10	0.82
CeN/CeN*		0.96	0.86	0.99	0.93	0.88	0.91	0.91	0.98	1.01	0.96	0.97	1.02
LOI (Lost of Ignition)													
Eu/Eu*	Eu-anomaly												
Ce/Ce*	Ce-anomaly												
N-normalised to PASS													

wide ranges: $\delta^{13}C$ from –5.04 to +2.63 ‰ VPDB, $\delta^{18}O$ from –7.03 to +2.49 ‰ VPDB associated both with facies and with environmental variability of the sequence.

The $\delta^{18}O$ vs. $\delta^{13}C$ variation chart documents the polymodal type of the data set but two main limestones and dolostones subgroups are distinctly separated (Fig. 17). The position of other points in the chart indicates more complex processes, mainly in the "transitional beds". The low $\delta^{18}O$ vs. $\delta^{13}C$ data covariance of the whole set and/or separated subgroups documents quite well preserved isotopic records of the carbonate beds and detects a transgression regime of sedimentation.

Discussion

REE distribution during transgression

The typical seawater REE pattern shows HREE enrichment, often also with negative Ce anomaly (Hannigan & Sholkovitz 2001; Haley et al. 2004; Ounis et al. 2008). The REE (III) — carbonate ion complexes are the dominant dissolved REE species in seawater: their ability to form carbonate complexes increases from light REE (LREE) to heavy REE (HREE). Increased REE accumulation could be more ef-

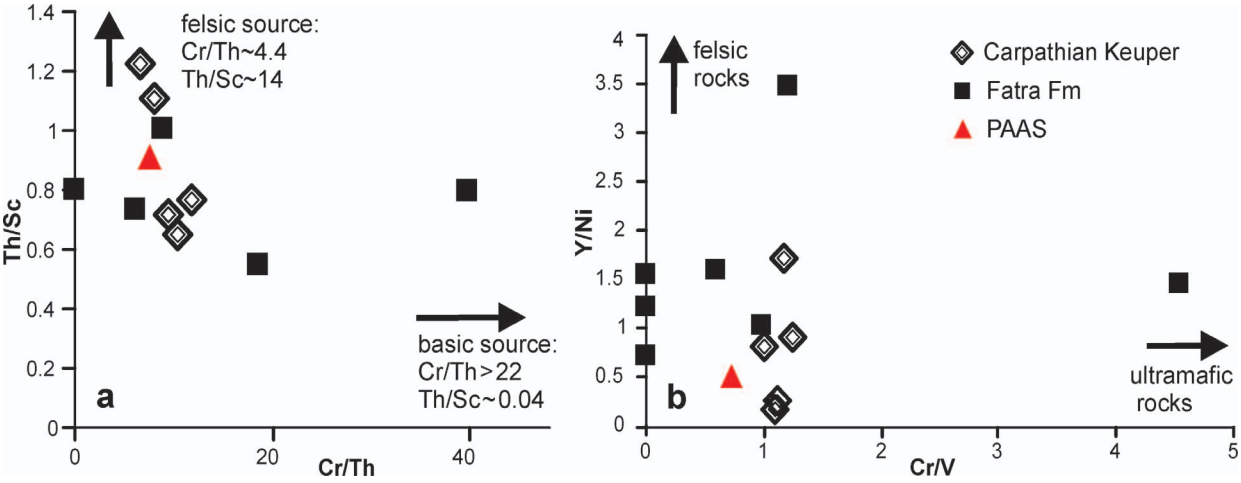

Fig. 14. Felsic/mafic sources of clastic material.

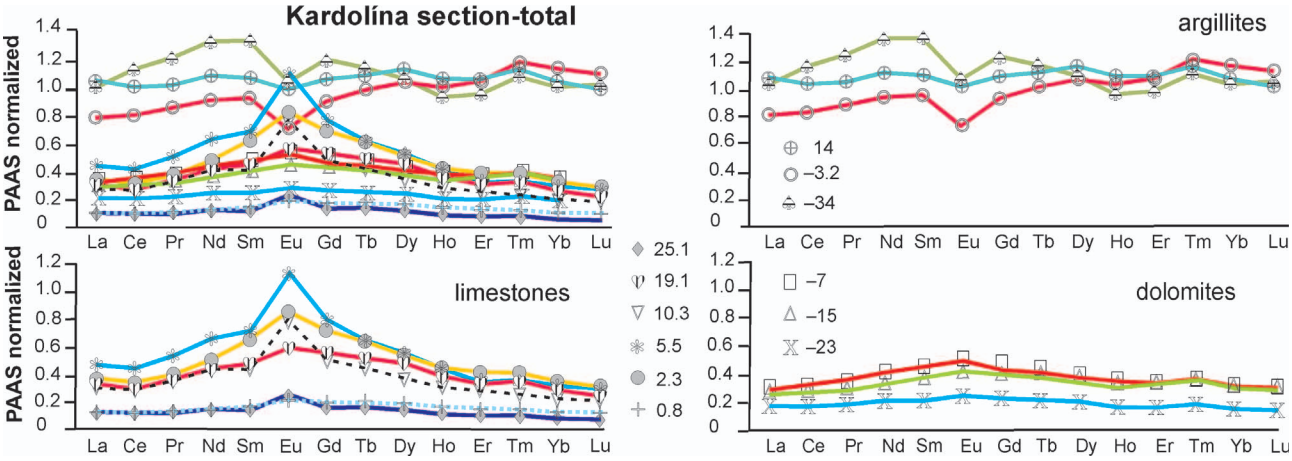

Fig. 15. REE contents in argillites, limestones and dolomites of the Kardolína section.

fective in the occurrence of biogenic apatite (like bonebed apatite) where Eu^{2+} or trivalent REE ions substitute Ca^{2+}. The REE released from iron oxides, from particulated organic matter (POC) and potentially from other active surfaces (clays) served as alternative source of REE in the carbonates precipitated (Haley et al. 2004; Shield & Webb 2004). Observed changes in REE content (or pattern; Table 1, Fig. 15) indicated a restoration of marine water composition during the transgression. However, the REE distribution in sediments could change due to fluctuation of redox and pH condition. Different dissolved species can be introduced or removed from the seawater and cause variation in the water and sediments (Ounis et al. 2008; Sheldon & Tabor 2009). The distribution of REE can also indicate weathering process, because their leaching behaviour varies according the regional humidity and increased acidity, as documented in paleosoils (Sheldon & Tabor 2009). Eu and Ce anomalies in REE distribution pattern commonly identify redox proxies, because Eu^{2+} separates from other REE^{3+} under reducing condition and Ce^{4+} divides into oxide under oxidizing conditions (Cao et al. 2012).

The different REE distribution patterns in the sample set studied indicate variability of the siliclastic source or unstable transport by wind and water flow during Carpathian Keuper dolostone and Fatra Formation limestone sedimentation. Eu enrichment in other REE indicates more reductive conditions during biogenic limestone precipitation or during early diagenesis, as relative increase of C_{org} contents (Fig. 16) indicates. However, biogenic carbonates are also enriched in phosphate, in which REE accumulated. The "bell-shaped" MREE-pattern could indicate that weathering of biogenic phosphates in freshwater could mobilize MREE and relatively increase its content in the limestone rock (Hannigan & Sholkovitz 2001; Ounis et al. 2008). Local bone-beds occurred in the basal part (Beds 0.4, 2.1, 2.2; Fig. 5) of the Fatra Formation.

Carbon isotope distribution during transgression

Negative $\delta^{13}C$ values in the Carpathian Keuper sequence (Beds -43 to 0) and also in the first two sedimentary cycles (IV/V) of the Fatra Formation (Beds +1 to +7: -3.25 to -0.59 ‰; Fig. 16) fluctuate between -0.05 and -5.0 ‰, but mostly in the range from -2 to -5 ‰. Later, in the sixth cycle, $\delta^{13}C$ values continually increase to positive $\delta^{13}C$ range (from

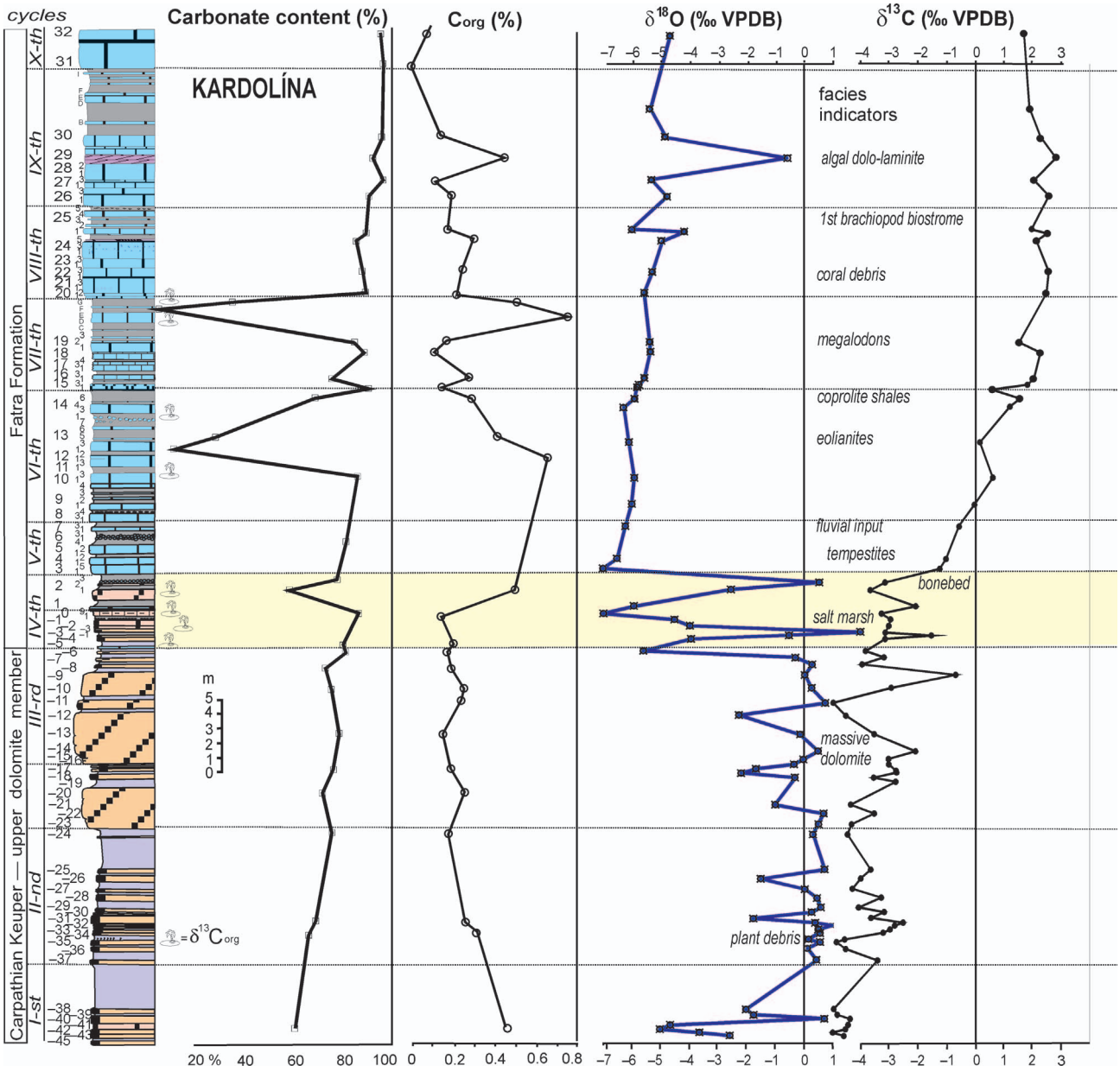

Fig. 16. Contents of organic carbon (TOC) and $\delta^{18}O$ and $\delta^{13}C$ curves in the lowermost part of the Kardolína section.

−0.05 to +1.22 ‰). These three cycles locate a span of temporal sedimentation and indicate continuing carbonate production and accumulation within marine transgression. Increased $\delta^{13}C$ (from 1.84 to 2.69 ‰) value fall into the typical interval of marine limestone documented earlier (Michalík et al. 2007) in the higher part of the Kardolína section. Positive $\delta^{13}C$ values in limestone could indicate balanced marine conditions, where "biological pump" supported effective carbonate production without increase of accumulation and/or burial of organic carbon as documented by low content of total organic matter in the samples (Fig. 16).

Negative $\delta^{13}C$ values in dolomite generally document C enrichment by light ^{12}C isotope in comparison with common marine carbonates. Such isotopically light C could have been produced by specific production or by biotic extinction in the water column or by release from methane buried in sediment. Negative C-isotope event could indicate regional or global climate change as documented in the T/J boundary beds elsewhere (Pálfy et al. 2001, 2007; Ward et al. 2007; Michalík et al. 2007, 2010; Preto et al. 2010). As $\delta^{13}C$ negative values are associated with dolostones, they must have been connected with dolomite precipitation (Masaryk & Lintnerová 1997; Warren 2000; Garcia del Cura et al. 2001; Berra et al. 2010).

Carpathian Keuper $\delta^{18}O$ values fall in the range −7.03 to +2.49 ‰ and are associated with facies differences (Fig. 17). Negative to positive $\delta^{18}O$ values in the range −1 to +3 ‰ are typical of massive dolostones of the third cycle. Samples with more negative values in the interval from −3 to −1 ‰ are discontinually located in certain parts of the cycle and probably indicate climatic/hydrologic changes and copy os-

cillation pattern in sediments. However, as the cyclostratigraphy study indicates, the isotope sample set is too small to verify this dependence.

Sharp negative $\delta^{18}O$ excursions occur in the basal part of the dolostone sequence (Beds –43 to –40: from –5.02 to –4.74) and in the first cycle of the Fatra Formation (from –7.05 to +2.03). In both parts, mixture of calcite/dolomite mineralogy occurs. These $\delta^{18}O$ changes can be either connected with sedimentary facies, or they reflect composition of lake/basinal water. Local climatic/hydrological changes controlled the amount of fresh or meteoric water input to the Carpathian Keuper's brackish lake and decreased $\delta^{18}O$ values. The $\delta^{18}O$ pattern of the Beds –4 to +2 (cycle IV) indicates more complex process induced by marine transgression, where short saline to freshwater floods occurred.

Although post-sedimentary alteration of this part cannot be entirely excluded, continual increase to more positive $\delta^{13}C$ values documents continual restoration of marine ramp and does not indicate any important diagenetic substitution of carbonate phases.

Limestone $\delta^{18}O$ values are relatively similar to each other and fall in the range from –4.33 to –6.23 ‰, as a common feature of uppermost Triassic marine limestones (Michalík et al. 2007). A more positive $\delta^{18}O$ excursion (–0.66 ‰) in Bed 29 was associated with early diagenetic dolomitization of algal mats (Fig. 16). It reflected a salinity increase rather than freshwater influx. This supposition is underlined by slight response of $\delta^{13}C$ values to this episodic dolomitization.

Dolomitization model

As mentioned above, $\delta^{18}O$ and $\delta^{13}C$ variation (Fig. 17) simply indicates heterogeneity of the sample set. In comparison with diagenetic marine dolostone (Smith & Dorobek 1993; Warren 2000; Wacey et al. 2007), dolostone data fall into unusual area of the plot because of negative $\delta^{13}C$ (–4 to –3 ‰ VPDB) and more positive $\delta^{18}O$ (in range from –1.5 to +1.0). Relatively positive $\delta^{18}O$ data indicate either freshwater or saline reservoir waters (or dolomite-forming fluids) and negative $\delta^{13}C$ values reflect input or generation of carbon enriched to light C, probable isotopically fractionated in biogenic/metabolic process (Pálfy et al. 2001). If we accept the sedimentary and microfacies character of the dolostone studied, then the C and O isotope and Sr contents indicate that Keuper fine-crystalline dolomite precipitated from brine or from pore water and can be compared with type B of the Coorong dolostone (Rosen et al. 1989; Warren 2000; Garcia del Cura et al. 2001; Wacey et al. 2007). Brine with optimal Mg/Ca ratio can be generated by microbial processes in specific climate and hydrology. The life activity of S reducing (SRB) and photosynthesizing bacteria was frequently discussed as a source of organic matter (Bechtel et al. 2007), consumers of sulphates and producers of CO_2 enriched to light ^{12}C. However, study of the Coorong dolostone did not confirm regular occurrence of isotopically light C (Wacey et al. 2007). Negative $\delta^{13}C$ values also occur in soil carbonates where the influence of meteoric waters which are in chemical equilibrium with atmospheric CO_2 (–7 ‰ PDB) cannot be excluded at all (Warren 2000). Model with equilibrated soil-water or water-atmospheric CO_2 could be alternatively applied to the isotope composition of limestone/dolomite mixed mineralogy (–43 to –41 or –6 to –1) where negative $\delta^{13}C$ (–4 to –3 ‰) values are attached to negative $\delta^{18}O$ (–4 to –5 ‰). A similar mixed marine-meteoric model of the Carnian to Norian Keuper dolostone generation was presented by Rychliński (2008) and Jaglarz (2010). A relatively high content of Sr in carbonates came more probably from brine water. This interpretation is in line with the facies character of the Carpathian Keuper dolostones as climatically induced sediments.

Cyclostratigraphic remarks

The thickness of the Fatra Formation sequence in the Kardolína section (107 meters) is three times greater than in other sections. This gives a reason to suppose that the sequence is more complete, formed by a more rapid sedimentary rate (60 mm/kyr) on a gentle submarine slope. 18 sedimentary cycles were distinguished in the Fatra Formation, which are attributable to short eccentricity (100 kyr) cycles, taking into consideration the 2 Myr duration of the Rhaetian; and three cycles have been discerned in the uppermost part of the Carpathian Keuper. The dominance of eccentricity cycles was stated during the Late Permian (cf. Legler & Scheider 2008); or during the Late Triassic/Early Jurassic (Haas et al. 2010). Both the geometry and lithological composition of the majority of the Fatra Formation cycles indicate a shallowing upward trend: however, this phenomenon was often combined with the effect of freshwater influx bringing coarse sedimentary particles (Fig. 18) in conditions of raised humidity trend at the end of the Triassic (Ahlberg et al. 2002; Preto et al. 2010).

Fine lamination preserved in the "zero interval" of the transitional (IV) cycle between the Carpathian Keuper and

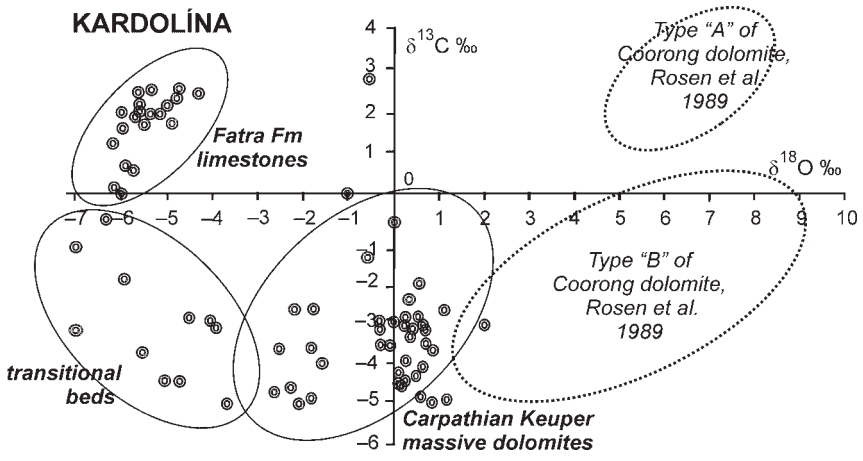

Fig. 17. Grouping of C and O isotopes in carbonates of the Kardolína section compared with typical composition of the Coorong dolomite.

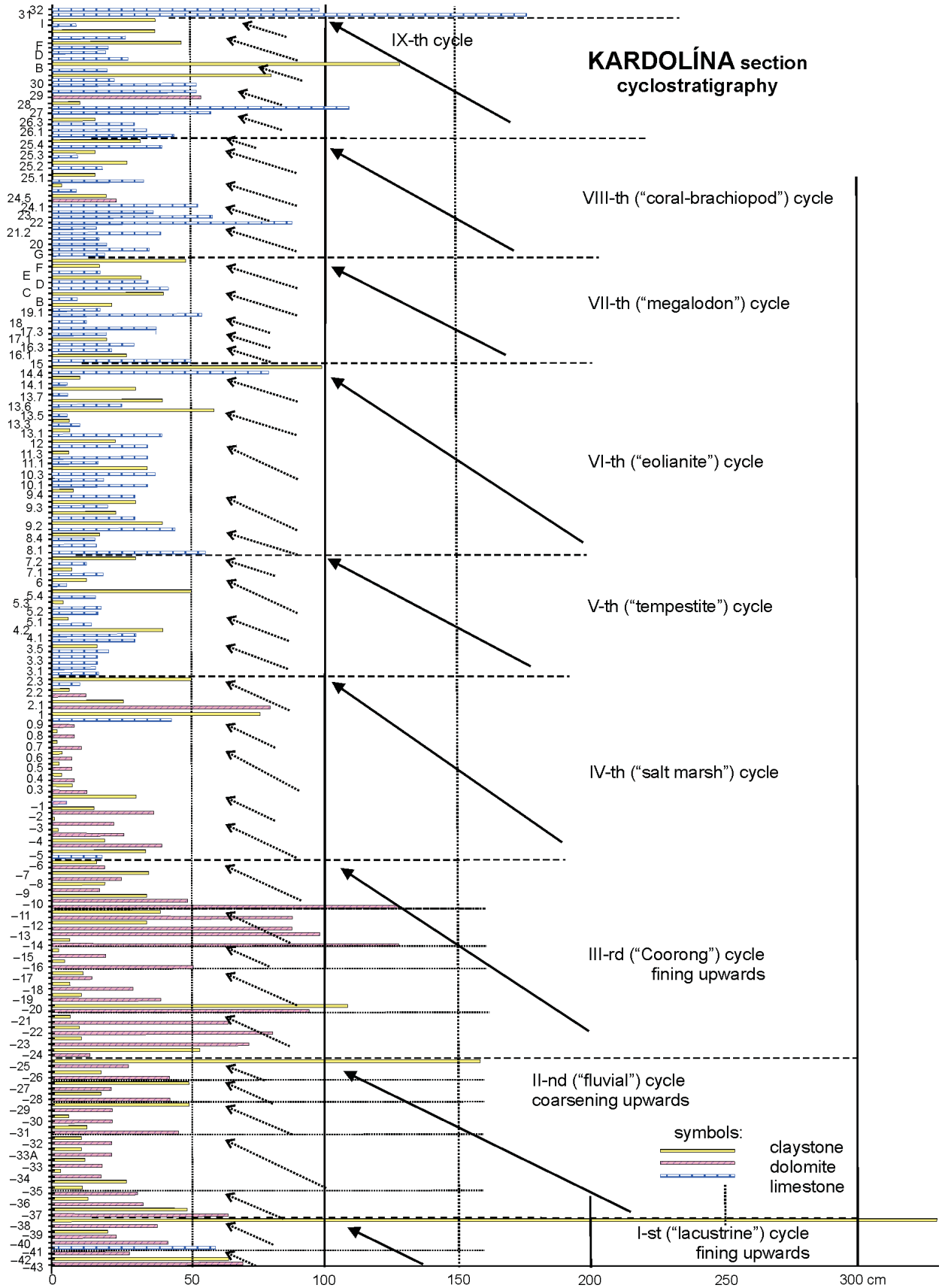

Fig. 18. Schematic illustration of cyclostratigraphic division of the Carpathian Keuper sequence in the Kardolína section based on bed thickness.

the Fatra Formation deserves special attention. Beds 0.3, 0.4, 0.5, 0.6 and 0.9 consist of argillite to marly mudstone. Detrital quartz forms 0.4 to 2.3 mm thick laminae. Individual laminae are arranged in a regular pattern (Fig. 19): two thicker bands are usually followed by seven thinner ones. Considering the average sedimentary rate, influx events bringing quartz detritus must have repeated in rhythms of approximately 20 years (solar Hale cycles?).

The close-up view on the dololaminite in Bed 29 (Fig. 19) is even more surprising. Laminae are well preserved, showing details of a fine stratification pattern. Several laminae show stromatolitic character of former algal mats. Planar laminae are very thin (0.2 to 0.8 mm), in bundles of 7 to 9 (=Hale rhythm?). In closer view, series of thinner laminae are visible between them, in groups of 5.

Magnetic susceptibility

According to Ellwood et al. (2000) and Crick et al. (2001), the MS record in most marine rocks is of detrital origin and related to the influx of lithogenic fraction to a basin, controlled by both: climate variations (e.g. humidity) and eustatic sea-level changes. MS highs and lows are related to regressive and transgressive intervals, respectively. The model seems to work in rather open marine environments (Whalen & Day 2010). However, in the carbonate platform settings an inverse correlation might also be observed (Da Silva et al. 2009). In the Kardolína section the lowest sea-level is postulated at the transition interval between the Carpathian Keuper and Fatra Formation. It corresponds well to MS trends observed in the Kardolína section. The Carpathian Keuper with increasing MS trend would correspond to the regressive interval, while stepwise decrease of MS in the Fatra Formation might be interpreted as a transgressive trend. This interpretation alone would be not sufficient because it might be possible that the decreasing MS trend is related to dilution of ferromagnetic particles in carbonate matrix, and thus to a possibly higher sedimentation rate. However, as the same trend is also inferred from sedimentological analysis (see above) and MS correlates quite well with some sedimentological features, like quartz grain size (Fig. 4), it might be accepted as a quite likely model.

The primary nature of the MS record might also be tested, correlating the MS values with Al_2O_3. Al is regarded as a predominantly lithogenic element which might be used as a proxy for fine detrital clay input into the basin (Calvert & Pedersen 1993; Śliwiński et al. 2010). The correlation graphs

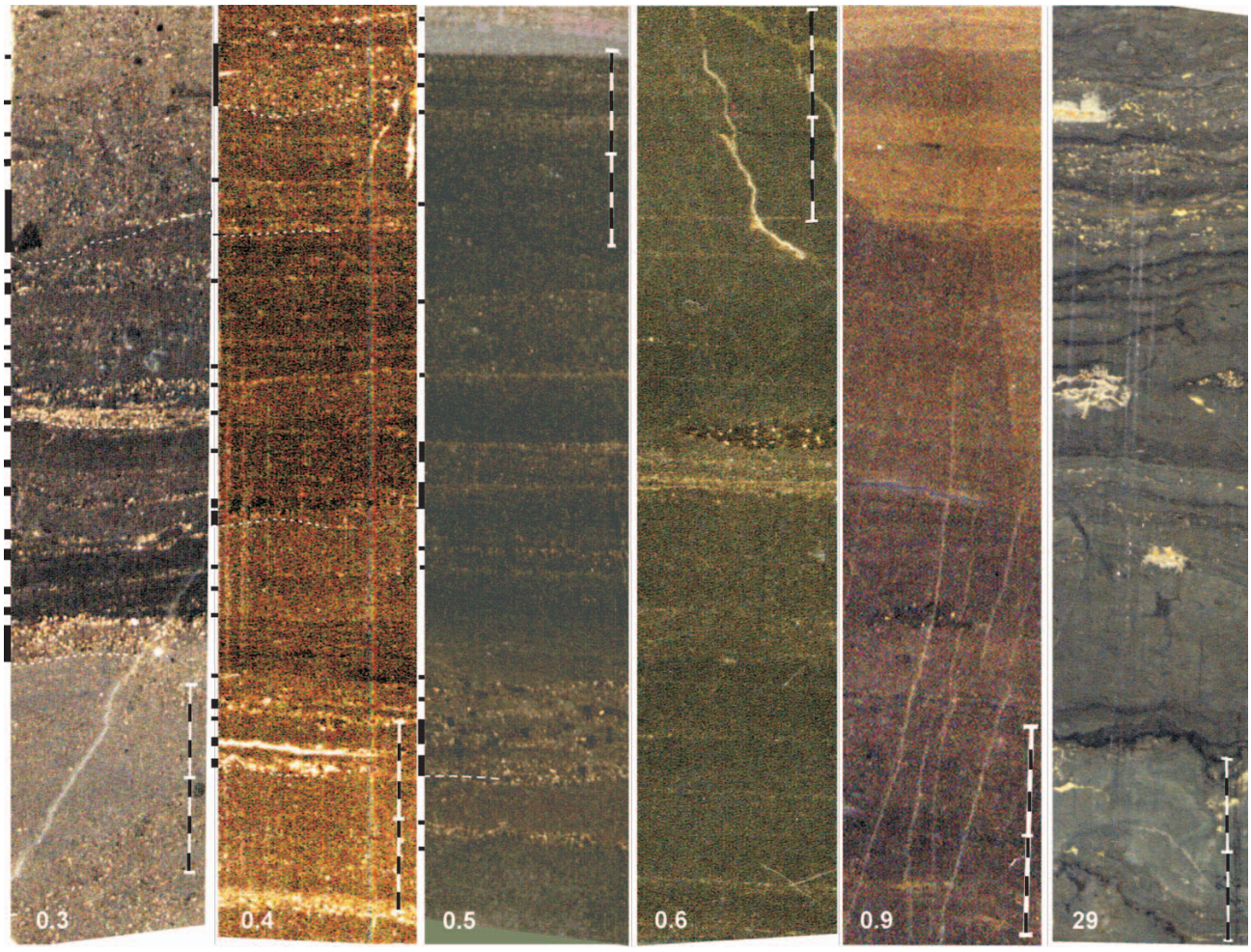

Fig. 19. Lamination in Beds 0.3, 0.4, 0.5, 0.6, 0.9 and 29, in the Kardolína section. Scale bars are 10 mm long.

(see Fig. 13e–f) reveal a moderate positive correlation between MS and Al content — this might be treated as preliminary confirmation that MS contains a significant detrital component. However, both MS and geochemical data were available from only 9 samples. Moreover, it seems that MS carriers are different in the Fatra Formation and Carpathian Keuper: the MS correlates with Al_2O_3 within a lithostratigraphic unit, but when the entire dataset is considered (Fatra Formation+Carpathian Keuper) — the correlation is not significant! It cannot be excluded that a part of the SP magnetite is of authigenic origin and not directly related to other erosion — derived components (Jackson 1993; Grabowski et al. 2009; Devleeschouwer et al. 2010).

Paleocommunities

The lowermost sedimentary cycles contain sporadic fossils, mostly plant fragments and ostracods, inhabiting temporal water reservoirs. The third cycle represents swampy environments which contained much more diverse mixed marine and brackish organisms: foraminifers (*Agathammina*), bivalve molluscs (*Rhaetavicula* community), linguloid brachiopods, sharks, fish, amphibians (?) and burrowing animals producing *Rhizocorallium* burrows.

The fifth cycle recorded stabilization of marine environments (and communities, cf. Michalík & Jendrejáková 1978; Gaździcki 1983) affected by storm activity. Inhabitants of shallow lagoons (*Corbula* and *Gervillaria* community) were periodically washed out by stormy turbulent waters from the soft bottom, killed and their broken shells were accumulated in tempestite layers. Shell accumulations formed temporary firm ground for an oyster (*Placunopsis*) community. During continuing deepening and accumulation of fine mud, the bottom was inhabited by an infaunal *Propeamussium* and *Entolium* community.

Fine quartz dust transported by eolian activity accumulated in a marine bay. Deteriorating oxygenation enabled deposition of shaly beds rich in coprolites, crinoid ossicles, pectinid bivalves and fish teeth. Megalodon limestone indicates settlement of pachyodont bivalves during shallowing events.

Conclusions

The Kardolína section yields an almost complete record of the Rhaetian marine transgression into the Zliechov Basin. A comprehensive study of mineralogy, lithology, lithostratigraphy, cyclostratigraphy, fossils, geochemistry including C and O stable isotopes and rock magnetism has provided detailed information about environmental changes at the end of the Triassic.

The sequence consists of distinct cycles of 100 kyr eccentricity and 40 kyr obliquity character, but some laminated layers also bear signs of much finer rhythmicity, including repetition in 100, 20 and even in 4(?) year cycles of events. Rhythmically repeating detrital laminae were formed by alternation of climatic parameters (monsoon-like periods). Analysis of clastic quartz grain size and content shows that both fluvial input and eolian activity were involved in their origin. On the other side, high concentrations of foraminifers (*Agathammina*) in some of these laminae indicates rather intensification of marine influence.

The sequence stratigraphic and cyclostratigraphic division fits well with magnetic susceptibility which reflects the distribution of authigenic and detrital constituents in the rock sequence. The good preservation of the primary magnetic record is promising from the point of view of magnetostratigraphic study which will be performed in the near future.

The integrated geochemical data are consistent with the character and time span of sedimentary facies evolution. C and O isotope curves responded selectively to changes of eustacy and climate and tightly followed restoration of marine carbonate ramp during the Rhaetian.

A wide range of $\delta^{18}O$ values (–7.0 to +2.7) by itself is not anomalous in the Triassic carbonates but combination of these data with negative $\delta^{13}C$ values resulted in an unusual distribution of dolostone data in the plot (Fig. 15, Table 1). It documents either dolomite precipitation from brackish or hypersaline lake water or its derivation from pore water comparable to the Recent Coorong B dolostone. Less positive $\delta^{18}O$ values indicate level of diagenetic/thermal fractionation of the oxygen isotope. Negative C values indicate water enrichment to light C (HCO_3^-) induced by microbial productivity.

Stabilization of benthic communities in the Fatra Formation basin was not straightforward since it was strictly controlled by physical environmental factors. Although foraminifers, bivalves and sharks appeared shortly after the start of the transgression, bivalve mollusc biostromes were repetitively destroyed by storms and temporary firm bottoms were colonized by oysters and burrowers. Bottom colonization by pachyodont bivalves, brachiopods and corals was possible much later, in highstand conditions.

Acknowledgments: The authors acknowledge help from three reviewers, namely Prof. József Pálfy for valuable discussion, inspiring comments and thorough corrections, but also Prof. Ján Soták and Dr. Tomasz Rychliński who substantially contributed to the scientific level of the manuscript. Field works could not have been done without the painstaking help of our young co-workers, namely Jakub Rantuch, Martin Závacký, Štefan Szalma, Mgr. Zuzana Weissová, Dr. Peter Ledvák, Dr. Martina Martincová, Mgr. Peter Klepsatel, Mgr. Ján Čatloš, and Mgr. Hanna Nizinkiewicz. We always met with friendly support from the Tatra National Park State Forests administration and its Research Station in Tatranská Lomnica (Dr. Stanislav Pavlarčík), and from the Spišská Belá municipality, as well. Field research was also supported by direction and workers of the Academia Hotel in Stará Lesná, where we always had our home base. Thanks for financial support go to 0065/12 VEGA Project. SEM photographs were provided by Dr. I. Holický (State Geological Institute of Dionýz Štúr, Bratislava) and by Mgr. N. Halašiová (Geological Institute SAS, Banská Bystrica). MS and rock magnetic experiments were performed within a Project No. 61.2301.0902.00.0 of the PGI-NRI, as a part of the IGCP 580 Project. Isotope analyses were done mostly by Dr. K. Małkowski (Polish Academy of Sciences, Warszawa).

References

Ahlberg A., Arndorf L. & Ohlson D. 2002: Onshore climatic change during the Late Triassic marine inundation of the Central European Basin. *Terra Nova* 14, 241–248.

Al-Juboury A.I. & Ďurovič V. 1992: Paleoenvironment interpretation of the Carpathian Keuper rocks as revealed by clay mineral analysis. *Geol. Carpathica, Clays* 2, 73–76.

Al-Juboury A.I. & Ďurovič V. 1996: Supratidal origin of Carpathian Keuper dolostones. *Miner. Slovaca* 28, 12–20.

Allasinaz A. 1972: Revisione dei Pettinidi triassici. *Riv. Ital. Paleont. Stratigr.* 78, 2, 189–428.

Bacelle L. & Bosellini A. 1965: Diagrammi per la stima visiva della composizione percentuale nelle rocce sedimentarie. *Ann. Univ. Ferrara, N. S., sez. IX., Sci. Geol. Paleont.* 1, 3, 59–62.

Bau M. & Dulski P. 1996: Distribution of yttrium and rare-earth elements in the Penge and Kuruman Iron-Formations, Transvaal Supergroup, South Africa. *Precambrian Res.* 79, 37–55.

Bechtel A., Gawlick H.-J., Gratzer R., Tomaselli M. & Püttmann W. 2007: Molecular indicators of palaeosalinity and depositional environment of small-scale basins within carbonate platforms. The Late Triassic Hauptdolomit Wiestalausee section near Hallein (N Calcareous Alps, Austria). *Organic Geochem.* 38, 92–111.

Berra F., Jadoul F. & Anelli A. 2010: Environmental control on the end of the Dolomia Principale (Hauptdolomit) depositional system in the Central Alps: coupling sea-level and climate change. *Palaeogeogr. Palaeoclimatol. Palaeoecol.* 290, 138–150.

Borza K. 1959: Geological and petrographical relationships of the Mesozoic sequences of the Belianske Tatry Mts and the Široká mountains group. *Geol. Sborn. SAV* 10, 133–182 (in Slovak).

Bromley R.G. 1996: Trace fossils, biology, taphonomy and applications. Second edition. *Chapman and Hall*, 1–361.

Cao J., Wu M., Chen Y., Hu K., Bian L., Wang L. & Zhang Y. 2012: Trace and rare element geochemistry of Jurassic mudstone in the northern Qaidam Basin, northwest China. *Chemie der Erde*., doi: 101016/j.chemer.2011.12.002

Cappetta H. 1987: Chondrichthyes II. Mesozoic and Cenozoic Elasmobranchii. *Handbook of Paleoichthyology* 3B, 1–193.

Condie K., Calvert S.E. & Pedersen T.F. 1993: Chemical composition and evolution of the upper continental crust: contrasting results from surface samples and shales. *Chem. Geol.* 104, 1–37.

Cox L.R. 1961: New genera and subgenera of Mesozoic Bivalvia. *Paleontology* 4, 4, 592–598.

Crick R.E., Ellwood B.B., Hassani A.E., Hladil J., Hrouda F. & Chlupáč I. 2001: Magnetosusceptibility event and cyclostratigraphy (MSEC) of the Pridoli — Lochkovian GSSP (Klonk, Czech Republic) and coeval sequences in the Anti-Atlas, Morocco. *Palaeogeogr. Palaeoclimatol. Palaeoecol.* 167, 73–100.

Cullers R.L. 2000: The geochemistry of shales, siltstones and sandstones of Pennsylvanian-Permian age, Colorado, USA: implications for provenance and metamorphic studies. *Lithos* 51, 181–203.

Da Silva A.-C., Mabille C. & Boulvain F. 2009: Influence of sedimentary setting on the use of magnetic susceptibility: examples from the Devonian of Belgium. *Sedimentology* 56, 1292–1306.

Devleeschouwer X., Petitclerc E., Spassov S. & Préat A. 2010: The Givetian-Frasnian boundary at Nismes parastratotype (Belgium): the magnetic susceptibility signal controlled by ferromagnetic minerals. *Geol. Belgica* 13, 351–366.

Duffin C.J. & Gaździcki A. 1977: Rhaetian fish remains from the Tatra Mountains. *Acta Geol. Pol.* 27, 3, 333–348.

Ellwood B.B., Crick R.E., Hassani A.E., Benoist S.L. & Young R.H. 2000: Magnetosusceptibility event and cyclostratigraphy method applied to marine rocks: detrital input vs. carbonate productivity. *Geology* 28, 1135–1138.

Forster Th., Evans M.E. & Heller F. 1994: The frequency dependence of low field susceptibility in loess sediments. *Geophys. J. Int.* 118, 636–642.

Garcia del Cura M.A., Calvo J.P., Ordóñez Jones B.F. & Cañaveras J.C. 2001: Petrographic and geochemical evidence for the formation of primary bacterially induced lacustrine dolomites: La Roda "white earth" (Pliocene, central Spain). *Sedimentology* 48, 897–915.

Gaździcki A. 1974: Rhaetian microfacies, stratigraphy and facial development in the Tatra Mts. *Acta Geol. Pol.* 24, 1, 17–96.

Gaździcki A. 1983: Foraminifers and biostratigraphy of Upper Triassic and Lower Jurassic of the Slovakian and Polish Carpathians. *Paleont. Pol.* 44, 109–169.

Gaździcki A. & Iwanow A. 1976: The diachronism of the Rhaetic and "Gresten" Beds in the Tatra Mts (West Carpathians). *Bull. Acad. Pol. Sci., Sér. Sci. de la Terre* 24, 2, 117–122.

Gaździcki A., Michalík J., Planderová E. & Sýkora M. 1979: An Upper Triassic–Lower Jurassic sequence in the Krížna Nappe (West Tatra Mts, Western Carpathians, Czechoslovakia). *Západ. Karpaty, Geol.* 5, 119–148.

German C.R., Holiday B.P. & Elderfield H. 1991: Redox cycling of rare earth elements in the suboxic zone of the Black Sea. *Geochim. Cosmochim. Acta* 55, 3553–3558.

Golebiowski R. 1991: Becken und Riffe der Alpinen Obertrias-Lithostratigraphie und Biofazies der Kössener Formation. *Exkursionen Jungpaläozoikum und Mesozoikum Österreichs, Österr. Paläont. Gesell.*, 79–119.

Grabowski J., Michalík J., Szaniawski R. & Grotek I. 2009: Synthrusting remagnetization of the Krížna nappe: high resolution palaeo- and rock magnetic study in the Strážovce section, Strážovské vrchy Mts, Central West Carpathians (Slovakia). *Acta Geol. Pol.* 59, 2, 137–155.

Haas J., Götz A.E. & Pálfy J. 2010: Late Triassic to Early Jurassic paleogeography and eustatic history of the NW Tethyan Realm: new insights from sedimentary and organic facies of the Csövár Basin (Hungary). *Palaeogeogr. Palaeoclimatol. Palaeoecol.* 291, 456–468.

Haley A.B., Klinkhammer P.G. & Mc Manus S.J. 2004: Rare earth elements in pore waters of marine sediments. *Geochim. Cosmochim. Acta* 68, 1265–1279.

Hallam A. 1981: The end-Triassic bivalve extinction event. *Palaeogeogr. Palaeoclimatol. Palaeoecol.* 35, 1–44.

Hannigan E.R. & Sholkowitz R.E. 2001: The development of middle rare earth in freshwater: weathering of phosphate minerals. *Chem. Geol.* 175, 495–508.

Hautmann M. 2001: Die Muschelfauna der Nayband-Formation (Obertrias, Nor-Rhät) des östlichen Zentraliran. *Beringeria H.* 29, 3–181.

Hölder H. 1990: Über die Muschelgattung *Placunopsis* (Pectinacea, Placunopsidae) in Trias und Jura. *Stuttgarter Beitr. Naturkunde, Serie B, Geol. Paläont.* 165, 1–63.

Ivimey-Cook H.C., Hodges P., Swift A. & Radley J.D. 1999: Bivalves. In: Swift A. & Martill D.M. (Eds.): Fossils of the Rhaetian Penarth Group. *Palaeont. Assoc.,* London, 83–127.

Jackson M., Rochette P., Fillion G., Banerjee S. & Marvin J. 1993: Rock magnetism of remagnetized Paleozoic carbonates: Lowe Temperature behaviour and susceptibility characteristics. *J. Geophys. Res.* 98, B4, 6217–6225.

Jaglarz P. 2010: Facies and sedimentary environment of the carbonate-dominated Carpathian Keuper from the Tatricum Domain: Results from the Dolina Smytnia Valley (Tatra Mts, Southern Poland). *Ann. Soc. Geol. Pol.* 80, 147–161.

Kollárová-Andrusovová V. & Kochanová M. 1973: Molluskenfauna des Bleskový prameň bei Drnava (Nor, Westkarpaten). *Vydav. SAV, Bratislava*, 1–215.

Korte C., Kozur H.W. & Veizer J. 2005: $\delta^{13}C$ and $\delta^{18}O$ values of

Triassic brachiopods and carbonate rock as proxies for coeval seawater and paleotemperature. *Palaeogeogr. Palaeoclimatol. Palaeoecol.* 226, 287–306.

Legler B. & Schneider J. 2008: Marine ingression into the Middle/Late Permian saline lake of the southern Permian Basin (Rotliegend, N Germany), possible linked to sea-level highstands in the Arctic Rift System. *Palaeogeogr. Palaeoclimatol. Palaeoecol.* 207, 102–114.

Limanowski M. 1903: Continental Permian and Triassic sediments in the Tatra Mts. *Pamietnik Towarzystwa Tatrzańskiego* 24, 140–176 (in Polish).

Masaryk P. & Lintnerová O. 1997: Diagenesis and porosity of the Upper Triassic carbonates of the pre-Neogene Vienna Basin basement. *Geol. Carpathica* 48, 6, 371–386.

Michalík J. 1975: Genus *Rhaetina* Waagen, 1882 (Brachiopoda) in the uppermost Triassic of the West Carpathians. *Geol. Zbor. Geol. Carpath.* 26, 1, 47–76.

Michalík J. 1977: Paläogeographische Untersuchungen der Fatra-Schichten (Kössen Formation) des N Teiles des Fatrikums in den Westkarpaten. *Geol. Zbor. Geol. Carpath.* 28, 1, 71–94.

Michalík J. 1978: To the paleogeographic, paleotectonic and paleoclimatic development of the West Carpathian area in the uppermost Triassic. In: Vozár J. (Ed.): Paleogeographic development of the Western Carpathians. *D. Štúr's Geol. Inst.,* Bratislava, 189–211.

Michalík J. 1979: Paleobiogeography of the Fatra Formation of the uppermost Triassic of the Western Carpathians. *Paleont. Konf. Univerzita Karlova, Praha 1978*, 25–39.

Michalík J. 1980: A paleoenvironmental and paleoecological analysis of the northern Tethyan nearshore region in the latest Triassic time. *Riv. Ital. Paleont. Stratigr.* 85, 3–4, 1047–1064.

Michalík J. 1982: Uppermost Triassic short-lived bioherm complexes in the Fatric, Western Carpathians. *Facies* 6, 129–146.

Michalík J. & Jendrejáková O. 1978: Organism communities and biofacies of the Fatra Formation (uppermost Triassic, Fatric) in the West Carpathians. *Geol. Zbor. Geol. Carpath.* 29, 1, 113–137.

Michalík J., Jendrejáková O. & Borza K. 1979: Some new Foraminifera species of the Fatra Formation (uppermost Triassic) in the West Carpathians. *Geol. Zbor. Geol. Carpath.* 30, 1, 61–91.

Michalík J., Lintnerová O., Gaździcki A. & Soták J. 2007: Record of environmental changes in the Triassic-Jurassic boundary interval in the Zliechov Basin, Western Carpathians. *Palaeogeogr. Palaeoclimatol. Palaeoecol.* 244, 71–88.

Michalík J., Biroň A., Lintnerová O., Götz A.E. & Ruckwied K. 2010: Climatic change at the T/J boundary in the NW Tethyan Realm (Tatra Mts., Slovakia). *Acta Geol. Pol.* 60, 535–548.

Mikuláš R. 2006: Ichnofabric and substrate consistency in Upper Turonian carbonates of the Bohemian Cretaceous Basin (Czech Republic). *Geol. Carpathica* 57, 2, 79–90.

Ounis A., Kocsis L., Chaabani F. & Pheifer H.-R. 2008: Rare earth elements and stable isotope geochemistry ($\delta^{13}C$ and $\delta^{18}O$) of phosphorite deposits in the Gafsa Basin, Tunisia. *Palaeogeogr. Palaeoclimatol. Palaeoecol.* 268, 1–18.

Pálfy J., Demény A., Haas J., Hetényi M., Orchard M.J. & Vetö I. 2001: Carbon isotope anomaly and other geochemical changes at the Triassic/Jurassic boundary from a marine section in Hungary. *Geology* 29, 11, 1047–1050.

Pálfy J., Demény A., Haas J., Carter E.S., Görög Á., Halász D., Oravecz-Scheffer A., Hetényi M., Márton E., Orchard M.J., Ozsvárt P., Vető I. & Zajzon N. 2007: Triassic–Jurassic boundary events inferred from integrated stratigraphy of the Csővár section, Hungary. *Palaeogeogr. Palaeoclimatol. Palaeoecol.* 244, 1, 11–33.

Preto N., Kustatscher E. & Wignall P.B. 2010: Triassic climate — state of the art and the perspectives. *Palaeogeogr. Palaeoclimatol. Palaeoecol.* 290, 1–10.

Reijmer J.J.G. 1998: Compositional variations during phases of progradation and retrogradation of a Triassic carbonate platform (Picco di Vallandro/Dürrenstein, Dolomites, Italy). *Geol. Rdsch.* 87, 436–448.

Roniewicz E. & Michalík J. 1998: Rhaetian scleractinian corals in the Western Carpathians. *Geol. Carpathica* 53, 3, 149–157.

Rosen M.R., Miser D.E., Starcher M.A. & Warren J.K. 1989: Formation of dolomite in the Coorong region, South Australia. *Geochim. Cosmochim. Acta* 53, 661–669.

Ruckwied K. & Götz A.E. 2009: Climate change at the Triassic/Jurassic boundary: palynological evidence from the Furkaska section (Tatra Mountains, Slovakia). *Geol. Carpathica* 60, 2, 139–149.

Rychliński T. 2008: Facies development and sedimentary environments of the Carpathian Keuper deposits from the Tatra Mts., Poland and Slovakia. *Ann. Soc. Geol. Pol.* 78, 1–18.

Seilacher A. 1954: Ökologie der triassischen Muschel *Lima lineata* (Schloth.) und ihrer Epöken. *Neu. Jb. Geol. Paläont., Monatshefte*, 4, 163–183.

Sheldon N.D. & Tabor N.J. 2009: Quantitative paleoenvironmental and paleoclimatic reconstruction using paleosols. *Earth Sci. Rev.* 95, 1–52.

Shields G.A. & Webb G.E. 2004: Has the REE composition of seawater changed over geological time? *Chem. Geol.* 204, 103–107.

Smith T.-M. & Dorobek S.L. 1993: Alteration of early-formed dolomite during shallow to deep burial: Mississippian Mission Canyon Formation, central to southwestern Montana. *Geol. Soc. Amer. Bull.* 105, 1389–1399.

Swift A. & Martill D.M. 1999: Fossils of the Rhaetian Penarth Group. *Palaeont. Assoc.,* London, 1–312.

Środoń J., Kotarba M., Biroň A., Such P., Clauer N. & Wójtowicz A. 2006: Diagenetic history of the Podhale — Orava Basin and the underlying Tatra sedimentary structural units (Western Carpathians): Evidence from XRD and K-Ar of illite–smectite. *Clay Miner.* 41, 751–774.

Todd J.A. & Palmer T.J. 2002: The Jurassic bivalve genus *Placunopsis*: New evidence on anatomy and affinities. *Palaeontology* 45, 3, 487–510.

Turnau-Morawska M. 1953: Carpathian Keuper, its petrography and sedimentology. *Acta Geol. Pol.* 3, 33–102 (in Polish).

Wacey D., Wright D.T. & Boyce A.J. 2007: A stable isotope study of microbial dolomite formation in the Coorong region, South Australia. *Chem. Geol.* 244, 155–174.

Ward P.D., Garrison G.H., Williford K.H., Kring K.H., Goodwin D., Beattie M. & McRoberts C. 2007: The organic carbon isotopic and paleontological record across the Triassic-Jurassic boundary at the candidate GSSP section at Fergusson Hill, Muller Canyon, Nevada, USA. *Palaeogeogr. Palaeoclimatol. Palaeoecol.* 244, 281–289.

Warren J. 2000: Dolomite: occurrence, evolution and economically important association. *Earth Sci. Rew.* 52, 1–81.

Whalen M.T. & Day J.E. 2010: Cross-basin variations in magnetic susceptibility influenced by changing sea level, paleogeography, and paleoclimate; Upper Devonian, Western Canada Sedimentary Basin. *J. Sed. Res.* 80, 1109–1127.

Winkler G.G. 1859: Die Schichten der Avicula contorta inner- und ausserhalb der Alpen: Paläontologisch-geognostische Studie. *Johann Palm Hofbuchhandlung,* Munchen, 1–51, 2 plates.